

Vitamin D supplementation ameliorates ductular reaction, liver inflammation and fibrosis in mice by upregulating TXNIP in ductular cells

Received: 7 June 2024

Accepted: 2 May 2025

Published online: 13 May 2025



Eun Bok Baek ^{1,2,10}, Hyuk Soo Eun ^{3,4,10}, Jun-Yeop Song ^{1,10}, Eun-Ju Hong¹, Se-Hee Park⁵, Poornima Kumbukghadeniya ¹, Sang-Min Park ⁶, Seok-Hwan Kim ⁷, Soon Ok Kim ⁸, Ha Neul Kim ⁸, Young-Eun Cho⁹, Young-Suk Won ⁵  & Hyo-Jung Kwon ¹ 

Ductular reaction is associated with liver disease progression, but there are no drugs targeting ductular reaction. Vitamin D deficiency is common in chronic liver diseases and related to disease progression, but the underlying mechanisms by which vitamin D regulates liver diseases progression remain unclear. Here, we show that vitamin D plasma levels are negatively correlated with the degree of ductular reaction in patients with chronic liver diseases. 1,25(OH)₂D₃, the active form of vitamin D, reduces 3,5-diethoxycarbonyl-1,4-dihydrocollidin (DDC)-induced ductular reaction, liver inflammation, and fibrosis in female mice and upregulates the vitamin D target gene, *TXNIP* (encoding thioredoxin-interacting protein), in ductular cells. Cholangiocyte-specific *Txnip*-knockout female mice are more susceptible to DDC-induced ductular reaction, inflammation, and fibrosis. Deletion of *Txnip* in cholangiocytes promotes proliferation and suppressed death. Furthermore, *Txnip* deficiency increases TNF- α and TGF- β secretion by cholangiocytes to stimulate Kupffer cells and hepatic stellate cells, consequently leading to inflammation and collagen deposition. Biliary *Txnip* deficiency abolishes the protective effects of vitamin D, and TXNIP overexpression attenuates DDC-induced ductular reaction and inflammation and fibrosis. Collectively, our findings identify new mechanism how vitamin D ameliorates liver diseases and suggest that the vitamin D/TXNIP axis is a therapeutic target for addressing ductular reaction and liver diseases.

Chronic liver diseases (CLDs), including viral hepatitis, alcohol-associated liver disease (ALD), metabolic dysfunction-associated steatotic liver disease (MASLD), primary biliary cholangitis (PBC), and primary sclerosing cholangitis (PSC), are associated with hepatocyte injury and varying degrees of inflammation and fibrosis that

predispose patients to developing hepatocellular carcinoma (HCC). CLDs can have distinct clinical presentations independent of their underlying cause, but most share the common feature of ductular reaction^{1,2}. Ductular reaction is defined as the proliferation of ductular reactive cells through the proliferation of pre-existing cholangiocytes,

differentiation of hepatic progenitor cells (HPCs), and/or biliary metaplasia of hepatocytes. The proliferated cells can exhibit a ductular phenotype and be identified with the cholangiocyte markers, cytokeratin (CK)19, CK7, and SRY-box transcription factor 9 (SOX9)³. Reactive ductular cells acquire novel functions, such as the secretion of cytokines, chemokines, and growth factors that enable them to establish intense paracrine communications with various liver cells. Ductular reactive cells induce portal infiltration of immune cells, such as macrophages and neutrophils, leading to portal inflammation^{4–6}. They are also associated with hepatic stellate cell (HSC) activation, leading to extra cellular matrix (ECM) secretion and liver fibrosis^{4,7}. In humans, the degree of ductular reaction is correlated with CLD severity and short-term mortality, regardless of the etiology^{8–10}.

Vitamin D is a systemic hormone that functions in calcium and phosphate homeostasis, and is essential for proper bone development and maintenance. It also regulates immune responses, fibrogenesis, and cell proliferation and differentiation¹¹. Vitamin D is generated from its precursor, cholecalciferol, to yield bioactive 25-hydroxyvitamin D₃ [25(OH)D₃] in the liver; this binds to vitamin D-binding-protein¹² for transport to the kidney, where it functions in its biologically active form, 1 α , 25-dihydroxyvitamin D₃ (1 α ,25(OH)₂D₃)¹³. Accumulating data indicate that vitamin D deficiency is frequent in CLDs^{14–17} and decreased serum 25(OH)D₃ is associated with liver inflammation and fibrosis^{18,19}. Studies showed that 1,25(OH)₂D₃ treatment exerts a pronounced anti-hepatic fibrosis effect through inhibiting the activation of HSCs^{20,21}, whereas vitamin D deficiency promotes Kupffer cells (KCs) infiltration in ALD²². However, the underlying molecular mechanisms through which vitamin D hinders the development of liver inflammation and fibrosis warrant further investigation.

The biological activity of 1,25(OH)₂D₃ depends on its binding to nuclear vitamin D receptor (VDR). Activated VDR heterodimerizes with retinoid X receptor (RXR), and this heterodimer binds to vitamin D-responsive elements in target gene promoters to regulate gene expression²³. Thioredoxin-interacting protein (TXNIP), a putative vitamin D target gene originally identified as vitamin D₃ upregulated protein 1 (VDUP1), is upregulated in the human HL-60 promyelocytic cell line by 1,25(OH)₂D₃ treatment²⁴. Vitamin D supplementation increases apoptotic cell death and induces cell-cycle arrest via upregulation of TXNIP^{25,26}. In HCC, the vitamin D-induced upregulation of TXNIP reduces cell proliferation and increases apoptosis²⁷, suggesting that TXNIP contributes to the protective effects of vitamin D against HCC development. Furthermore, TXNIP expression is upregulated in patients with ALD and MASLD, and TXNIP attenuates ethanol-induced liver injury and methionine choline-deficient (MCD) diet-induced steatohepatitis^{28,29}.

Here, we explored the effects of vitamin D on ductular reaction and CLDs, and investigated underlying mechanisms. Our data reveal that vitamin D supplementation ameliorates ductular reaction and reduces liver inflammation and fibrosis largely through TXNIP.

Results

In patients with CLDs, vitamin D plasma levels negatively correlate with ductular reaction severity

Vitamin D deficiency is frequently noted in patients with CLDs, and ductular reaction is highly correlated with CLD progression^{7,18,19}. Here, to evaluate the significance of vitamin D in ductular reaction and CLDs, we analyzed a cohort of 114 patients with CLDs of various etiologies. Vitamin D plasma levels were reduced in patients with CLDs of all examined etiologies, including chronic viral hepatitis B (HBV; *n* = 53), alcohol (*n* = 24), PBC (*n* = 7), metabolic dysfunction-associated steatohepatitis (MASH; *n* = 13), and unidentified (*n* = 17) (Fig. 1A, B). To evaluate the clinical significance of the decreased vitamin D levels, we examined the associations with the clinical characteristics and liver histopathological features of patients with CLDs. Indeed, vitamin D levels were negatively correlated with

hepatic biochemical parameters, including alanine aminotransferase (ALT), aspartate aminotransferase (AST), total bilirubin (T-bilirubin), international normalized ratio (INR), and Child-Pugh score (Fig. S1), and negatively related with fibrosis stage (Fig. 1C). However, there was no significant difference in vitamin D levels between early (stage 1–2) and advanced (stage 4) fibrosis (Fig. 1D).

Many more pan-CK⁺ and SOX9⁺ cells were observed around portal areas of patients with CLDs compared to control individuals (Fig. 1E) and in patients with CLDs of all examined etiologies compared to control individuals (Fig. 1F, G). The numbers of pan-CK⁺ and SOX9⁺ cells were positively correlated with hepatic biochemical parameters and higher in patients with more advanced fibrosis (Fig. 1H and Fig. S2). In contrast, vitamin D plasma levels were negatively correlated with the numbers of pan-CK⁺ and SOX9⁺ cells (Fig. 1I), especially in patients with CLDs arising from HBV and alcohol (Fig. S3). These results suggest that the vitamin D plasma level is decreased in patients with CLDs and negatively correlates with the degree of ductular reaction.

1,25(OH)₂D₃ ameliorates ductular reaction and hepatic inflammation and fibrosis

To explore the role of vitamin D in ductular reaction and CLDs, mice were fed for 4 weeks with a 3,5-diethoxycarbonyl-1,4-dihydrocollidin (DDC) diet supplemented with or without 1,25(OH)₂D₃. DDC is a biliary toxicant that induces profound ductular reaction with hepatoperiductal fibrosis and massive portal/periportal inflammatory cell infiltration, which are key features of CLD^{4,30}. As expected, DDC feeding induced ductular reaction and expansion of pan-CK⁺ cells in mice. Meanwhile, 1,25(OH)₂D₃ treatment significantly reduced the numbers of pan-CK⁺ and proliferating pan-CK⁺BrdU⁺ cells (Fig. 2A). The hepatic expression levels of *Krt19*, *Krt7*, and *Sox9* were lower in 1,25(OH)₂D₃-treated versus vehicle-treated mice (Fig. 2B). 1,25(OH)₂D₃-treated mice also exhibited fewer F4/80⁺ cells and decreased Sirius red-positive area (Fig. 2C). Quantitative real-time PCR (qPCR) analysis showed that the hepatic expression levels of genes involved in inflammation (tumor necrosis factor- α [*Tnf*] and adhesion G protein-coupled receptor E1 [*Adgre1*]) and fibrosis (transforming growth factor- β [*Tgfb1*], collagen 1 α 1 [*Col1a1*], collagen 3 α 1 [*Col3a1*], collagen 4 α 1 [*Col4a1*], tissue inhibitor of metalloproteinases-1 [*Timp1*], and matrix metalloproteinase 9 [*Mmp9*]) were markedly downregulated in 1,25(OH)₂D₃-treated mice (Fig. 2D, E). We also performed bile duct ligation (BDL), which robustly stimulates ductular reaction and serves as a mouse ductular reaction model^{4,30}. Consistent with our results obtained in the DDC diet model, BDL-induced ductular reaction and hepatic inflammation and fibrosis were reduced in 1,25(OH)₂D₃-treated mice (Figure S4). These results indicate that vitamin D supplementation could reduce ductular reaction and hepatic inflammation and fibrosis in mice.

1,25(OH)₂D₃ increases TXNIP expression in ductular epithelial cells

Vitamin D is reported to have effects on hepatic nonparenchymal cells, such as cholangiocytes, HSCs, liver macrophages, and liver sinusoidal endothelial cells (LSECs)³¹. To evaluate which hepatic cell types are vitamin D targets in our models, we isolated hepatocytes, cholangiocytes, HSCs, liver macrophages, and LSECs from mice that received standard rodent chow diet plus vehicle, DDC plus vehicle, or DDC plus 1,25(OH)₂D₃. Consistent with previous studies^{20,21}, 1,25(OH)₂D₃ treatment downregulated the DDC diet feeding-induced increases in the expression levels of actin alpha 2, smooth muscle, aorta (*Acta2*), *Col1a1*, *Col3a1*, and *Col4a1* in HSCs, and those of *Tnf*, interleukin 6 (*Il6*), and *Il1b* in liver macrophages (Figure S5). Furthermore, the DDC diet feeding-induced upregulations of proliferating cell nuclear antigen (*Pcna*), *Tnf*, and *Tgfb1* were significantly reduced, whereas that of caspase-3 (*Casp3*) was significantly increased in cholangiocytes from 1,25(OH)₂D₃-treated mice (Fig. 3A). However, in DDC-fed mice, 1,25(OH)₂D₃ treatment had no effect on hepatocytes proliferation and

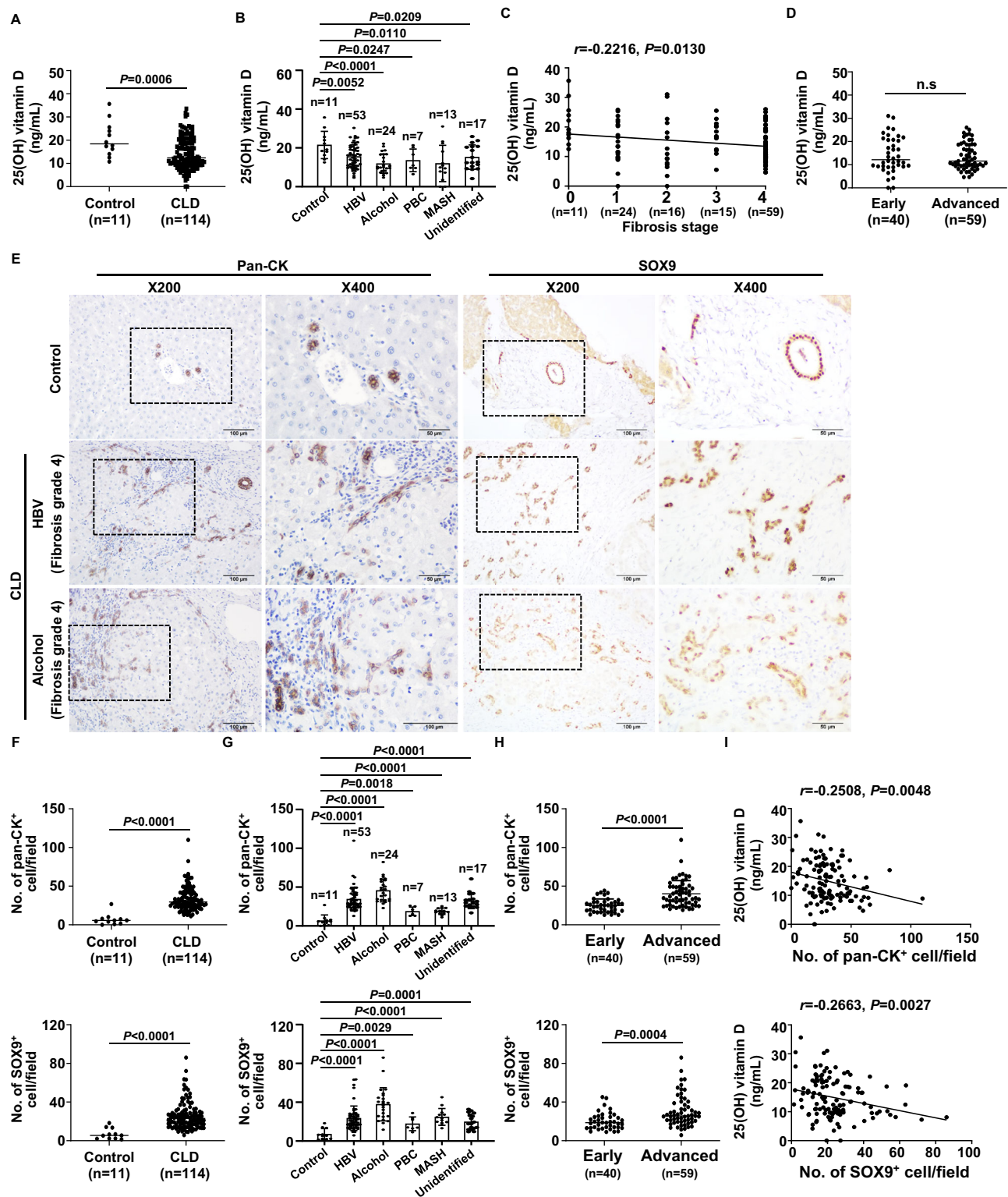


Fig. 1 | Vitamin D levels are decreased in CLDs and negatively correlated with the degree of ductular reaction. **A** Plasma levels of 25(OH) vitamin D in control individuals ($n=11$) and patients with CLDs ($n=114$). **B** Vitamin D plasma levels in control individuals ($n=11$) and patients categorized by CLD etiology, including HBV ($n=53$), alcohol ($n=24$), PBC ($n=7$), MASH ($n=13$), and unidentified ($n=17$). **C** Correlation between 25(OH) vitamin D levels and fibrosis stage (F0, $n=11$; F1, $n=24$; F2, $n=16$; F3, $n=15$; F4, $n=59$). **D** 25(OH) vitamin D levels in patients with early (stage 1-2, $n=40$) versus advanced (stage 4, $n=59$) fibrosis. **E** Representative IHC staining images of pan-CK and SOX9 in liver sections from control individuals and patients with CLDs. Original magnifications: 200X and 400X. **F** The numbers of

pan-CK⁺ and SOX9⁺ cells in livers from patients with CLDs. **G** The numbers of pan-CK⁺ and SOX9⁺ cells in livers from patients with CLDs of various etiology. **H** Numbers of pan-CK⁺ and SOX9⁺ cells in samples categorized as early versus advanced fibrosis. **I** Correlation of pan-CK⁺ and SOX9⁺ cell numbers with 25(OH) vitamin D levels ($n=125$). Values represent means \pm SDs. *n.s.*, not significant. Significance determined by unpaired two-tailed *t* test (**A**, **B**, **D**, **F**, **G**, **H**). Correlations were assessed by Pearson correlation coefficient and line of best-fit was generated by simple linear regression analysis (**C**, **I**). Source data are provided as a Source Data file.

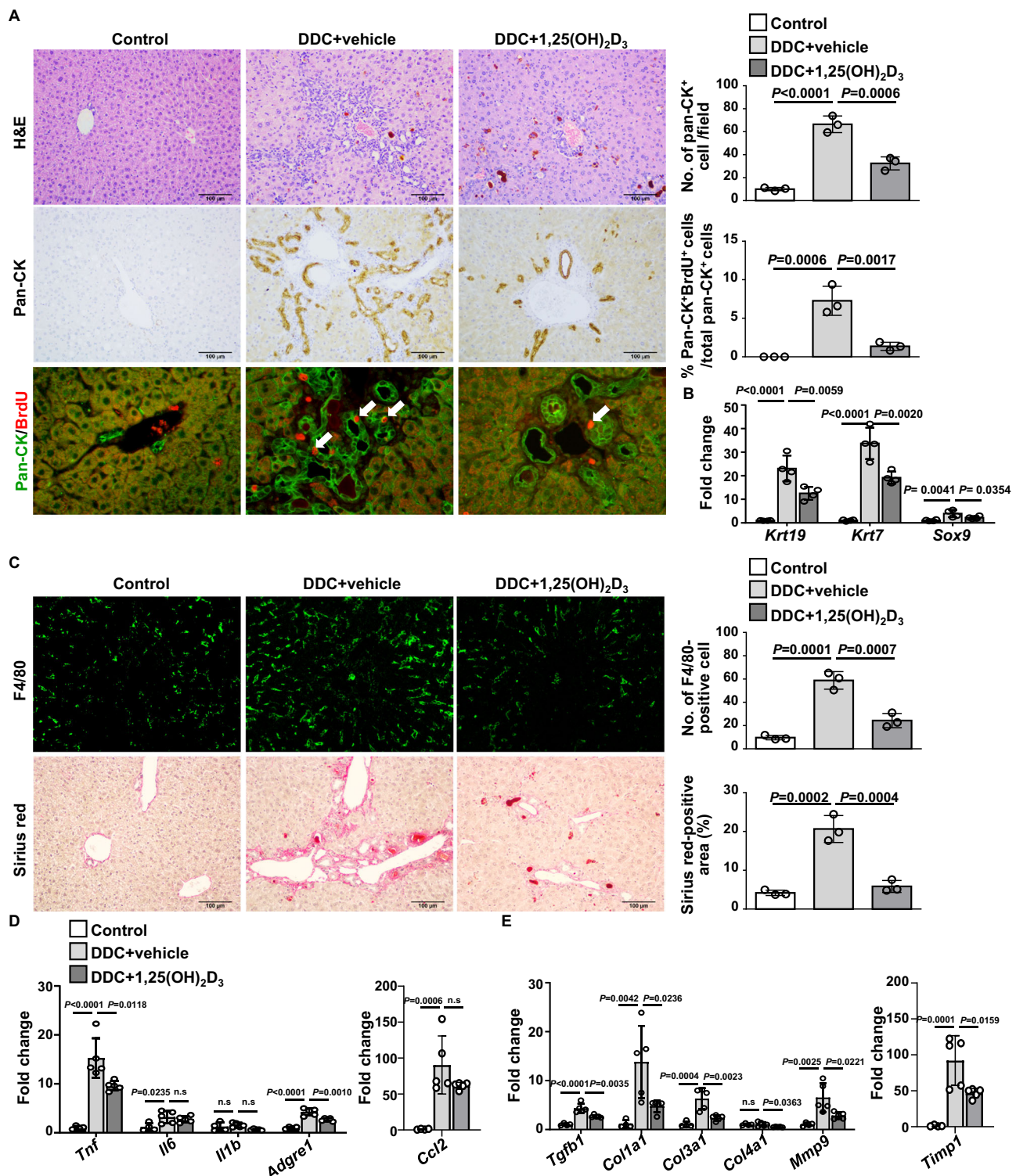


Fig. 2 | 1,25(OH)₂D₃ treatment prevents DDC-induced ductular reaction and liver inflammation and fibrosis. Female C57BL/6 mice were fed DDC diet for 4 weeks with or without 1,25(OH)₂D₃ treatment (5 µg/kg, 2x week). **A** Representative images of H&E staining, IHC staining for pan-CK, and IF staining for pan-CK/BrdU in normal chow diet-fed (control), DDC plus vehicle-treated, and DDC plus 1,25(OH)₂D₃-treated mice. Right: The numbers of pan-CK⁺ cells and pan-CK⁺BrdU⁺ cells ($n = 3$ /group). Original magnifications: 200X and 400X. **B** Hepatic mRNA levels

of *Krt19*, *Krt7*, and *Sox9* ($n = 4$ /group). **C** IF staining for F4/80 and Sirius red staining. Right: F4/80⁺ cell numbers and Sirius red-positive areas ($n = 3$ /group). Original magnification: 200X. Hepatic expression levels of genes involved in inflammation (**D**) and fibrosis (**E**) (Control, $n = 4$; DDC+vehicle, $n = 5$; DDC + 1,25(OH)₂D₃ $n = 5$). Values represent means \pm SDs. n.s., not significant. Significance determined by one-way ANOVA followed by Tukey's multiple comparisons test. Source data are provided as a Source Data file.

apoptosis (*Pcna*, B-cell lymphoma-2 [*Bcl2*], Bcl-2-associated X protein [*Bax*], and *Casp3*) and LSECs differentiation (Stabilin-1 [*Stab1*], Stabilin-2 [*Stab2*], platelet endothelial cell adhesion molecule 1 [*Pecam1*], and *Cd34*) (Fig. S5). The biological activity of vitamin D is known to be

mediated through VDR, which is expressed strictly in nonparenchymal cells of the liver^{31,32}. Here, we found that *Vdr* expression was increased in cholangiocytes (140.9-fold), HSCs (4.9-fold), and liver macrophages (1.3-fold) of 1,25(OH)₂D₃-treated mice, but unaltered in LSECs (Fig. 3B).

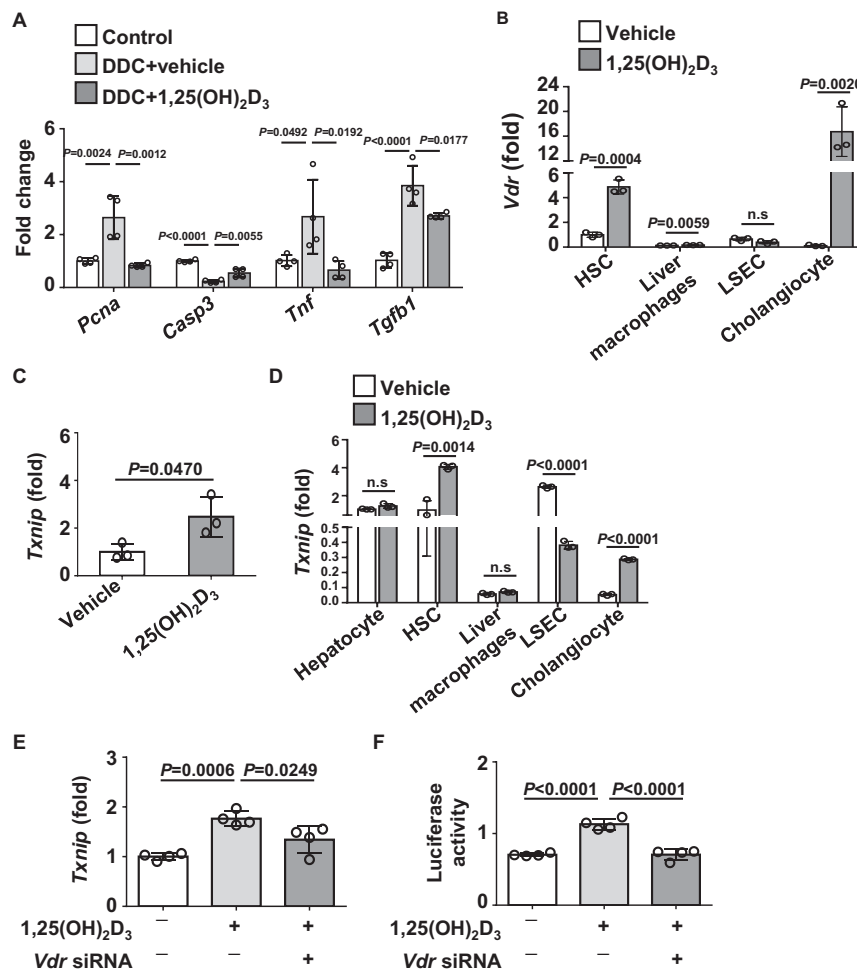


Fig. 3 | 1,25(OH)₂D₃ increases TXNIP expression in ductular cells. **A** The expression levels of *Pcn*, *Casp3*, *Tnf*, and *Tgfb1* in cholangiocytes. Female C57BL/6 mice were fed DDC diet for 4 weeks with vehicle or 1,25(OH)₂D₃ (5 µg/kg, 2x week) treatment and primary cholangiocytes were isolated ($n = 4$ /group). **B** Relative mRNA levels of *Vdr*. Female C57BL/6 mice were treated with 1,25(OH)₂D₃ (5 µg/kg, 2x week) for 4 weeks, and primary cholangiocytes, HSCs, liver macrophages, and LSECs were isolated ($n = 3$ /group). **C** Hepatic mRNA levels of *Txnip*. Female C57BL/6 mice were treated with 1,25(OH)₂D₃ (5 µg/kg, 2x week) for 4 weeks ($n = 3$ /group). **D** Relative mRNA levels of *Txnip*. Female C57BL/6 mice were treated with

1,25(OH)₂D₃ (5 µg/kg, 2x week) for 4 weeks, and primary hepatocytes, cholangiocytes, HSCs, liver macrophages, and LSECs were isolated ($n = 3$ /group). **E** qPCR analysis. BMOL cells were pre-incubated with control or *Vdr* siRNA for 24 h and treated with 1,25(OH)₂D₃ (10 µM) for 24 h ($n = 4$ biological replicates). **F** Luciferase assay. BMOL cells were pre-incubated with control or *Vdr* siRNA for 24 h and treated with 1,25(OH)₂D₃ (10 µM) for 6 h ($n = 4$ biological replicates). Values represent means \pm SDs. n.s., not significant. Significance determined by one-way ANOVA followed by Tukey's multiple comparisons test (**A**, **E**, **F**) and unpaired two-tailed *t* test (**B**, **C**, **D**). Source data are provided as a Source Data file.

These results indicate that the hepatoprotective effects of vitamin D supplementation could be mediated by cholangiocytes, HSCs, and liver macrophages.

Given that *TXNIP* is a vitamin D target gene^{25–27}, we examined whether vitamin D could regulate *TXNIP* expression in liver. Indeed, 1,25(OH)₂D₃ treatment increased the hepatic mRNA level of *Txnip* in mice (Fig. 3C). To determine the origin of this TXNIP, we isolated hepatocytes, cholangiocytes, HSCs, liver macrophages, and LSECs from vehicle- and 1,25(OH)₂D₃-treated mice. In the vehicle-treated mice, the major *Txnip*-expressing cells were hepatocytes, HSCs, and LSECs. In 1,25(OH)₂D₃-treated mice, the *Txnip* mRNA levels were markedly altered in cholangiocytes (5.3-fold increase), HSCs (4.2-fold increase), and LSECs (6.9-fold decrease) (Fig. 3D). TXNIP and VDR were upregulated in both cholangiocytes and HSCs of vitamin D-treated mice. This finding, along with previous reports that vitamin D exerts anti-hepatic fibrosis and anti-inflammatory effects through regulating HSCs and macrophages^{33–35}, prompted us to herein focus on how vitamin D impacts cholangiocytes. When BMOL cells, a well-defined mouse ductular cell/HPC line, and human cholangiocyte MMNK-1 cells were treated with 1,25(OH)₂D₃, TXNIP expression was upregulated

(Fig. S6A–C). 1,25(OH)₂D₃-induced TXNIP upregulation in BMOL cells was significantly blocked by pre-treatment with *Vdr* siRNA (Fig. 3E and Fig. S6D, E) and a luciferase reporter gene assay showed that 1,25(OH)₂D₃ significantly enhanced *Txnip* promoter activity, whereas introduction of *Vdr* siRNA inhibited this effect (Fig. 3F). These results demonstrate that vitamin D acts through VDR to transcriptionally activate the *Txnip* promoter in ductular cells.

Cholangiocyte-specific *Txnip* deletion exacerbates ductular reaction and liver inflammation and fibrosis in DDC-fed mice

To determine the role of vitamin D-induced TXNIP upregulation in ductular epithelial cells, we generated tamoxifen-induced cholangiocyte-specific *Txnip*-deficient (*Txnip*^{fl/fl}*Sox9-CreER*⁺; hereafter referred to as *Txnip*^{ΔSox9}) mice by crossing *Txnip*^{fl/fl} mice with *Sox9-CreER* mice. The knockdown of TXNIP in cholangiocytes was confirmed by qPCR and double immunofluorescence staining for pan-CK and TXNIP (Fig. S7). DDC-fed *Txnip*^{ΔSox9} mice formed many large bile ducts near portal regions, as demonstrated by the appearance of oval-shaped cells on hematoxylin and eosin (H&E) staining and the accumulation of pan-CK⁺ cells (Fig. 4A, B). Interestingly, DDC-fed *Txnip*^{ΔSox9} mice exhibited

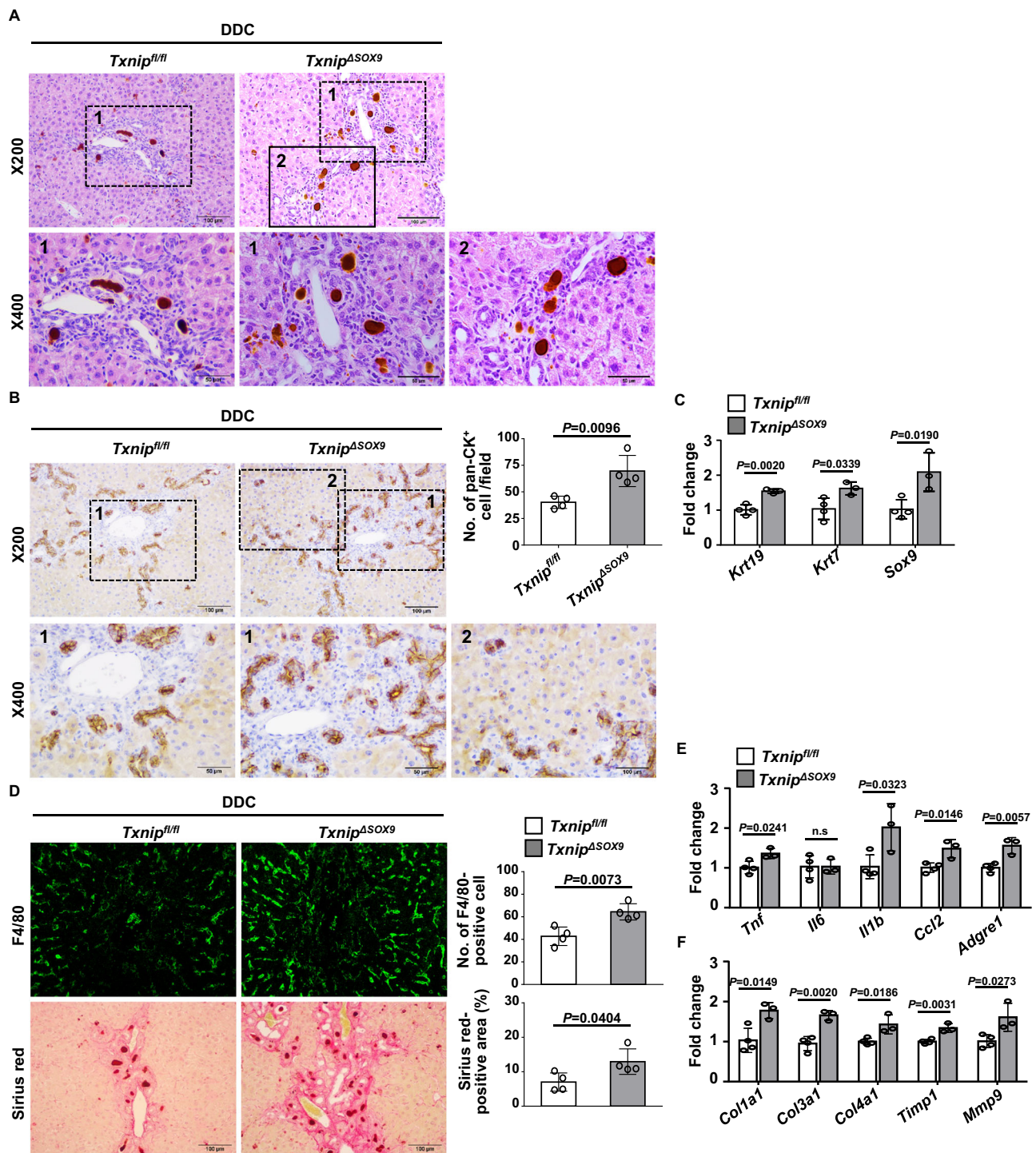


Fig. 4 | *Txnip* deficiency in cholangiocytes exacerbates ductular reaction and liver inflammation and fibrosis in DDC-fed mice. Female *Txnip^{fl/fl}* and *Txnip^{ΔSOX9}* mice were fed DDC diet for 4 weeks. **A** Representative H&E staining (*n* = 4/group). **B** IHC staining for pan-CK. Right: Numbers of pan-CK⁺ cells (*n* = 4/group). **C** Relative hepatic mRNA levels of *Krt19*, *Krt7*, and *Sox9* (*Txnip^{fl/fl}*, *n* = 4; *Txnip^{ΔSOX9}*, *n* = 3). **D** IF

staining for F4/80 and Sirius-red staining. Right: The F4/80⁺ cell numbers and Sirius red-positive areas (*n* = 4/group). Magnification: 200X. **E**, **F** qPCR analysis of genes involved in inflammation (**E**) and fibrosis (**F**) (*Txnip^{fl/fl}*, *n* = 4; *Txnip^{ΔSOX9}*, *n* = 3). Values represent means ± SDs. n.s., not significant. Significance determined by unpaired two-tailed t test. Source data are provided as a Source Data file.

massive ductular reaction in parenchymal regions and near portal regions (Fig. 4A, B). Pan-CK⁺ cells were significantly more numerous in DDC-fed *Txnip^{ΔSOX9}* mice compared to DDC-fed *Txnip^{fl/fl}* mice (Fig. 4B). qPCR showed that the hepatic levels of *Ck19*, *Ck7*, and *Sox9* were increased in DDC-fed *Txnip^{ΔSOX9}* mice (Fig. 4C). These results indicate that *Txnip* deletion in cholangiocytes promotes DDC-induced ductular reaction in vivo.

We further evaluated the contributions of TXNIP to liver inflammation and fibrosis. DDC-fed *Txnip^{ΔSOX9}* mice showed a higher degree of inflammation (the number of F4/80-positive cells and expression levels of *Tnf*, *Il1b*, and C-C motif chemokine ligand 2 [*Ccl2*], and *Adgre1*) and fibrosis (the Sirius red-positive area and expression levels of *Col1a1*, *Col3a1*, *Col4a1*, *Timp1*, and *Mmp9*) (Fig. 4D–F). Overall, these data indicate that cholangiocyte-specific deletion of *Txnip* likely

increases the susceptibility to DDC-induced ductular reaction and hepatic inflammation and fibrosis.

Biliary *Txnip* deficiency promotes cholangiocyte proliferation while suppressing cholangiocyte death

To directly evaluate the regulatory functions of TXNIP in ductular reaction, we performed RNA sequencing (RNA-seq) analysis in BMOL cells stably overexpressing *Txnip* (Fig. S8A). Principal component analysis (PCA) showed that *Txnip*-overexpressing cells were clearly separated from vector control cells (Fig. 5A). We identified 4,507 differently expressed genes (DEGs; 2,010 upregulated and 2,497 downregulated) in *Txnip*-overexpressing BMOL cells (Fig. 5B). Gene ontology (GO) analysis based on the Database for Annotation, Visualization, and Integrated Discovery (DAVID) database indicated that the DEGs seen under TXNIP overexpression were mainly enriched in apoptosis- and cell proliferation-related pathways (Fig. 5C). A heatmap revealed that TXNIP overexpression downregulated pro-proliferation- and anti-apoptosis-associated genes, and upregulated anti-proliferation- and pro-apoptosis-associated genes (Fig. 5D). Flow cytometric analysis further revealed that the percentages of cells in S phase and early apoptosis were lower and higher, respectively, in *Txnip*-overexpressing BMOL cells compared to vector controls (Fig. S8B). TXNIP overexpression also downregulated PCNA and B-cell lymphoma-extra-large (Bcl-xL) (Fig. S8C). In contrast, *Txnip* knockdown increased the S-phase cell percentage, PCNA expression, and Bcl-xL expression, but reduced the early apoptotic cell percentage and Bax expression (Fig. 5E and Fig. S9). To test whether vitamin D regulates cholangiocyte proliferation and apoptosis via TXNIP, we treated vitamin D in shRNA control and shRNA *Txnip* BMOL cells. Our results revealed that 1,25(OH)₂D₃ treatment downregulated the expression levels of PCNA and Bcl-xL and upregulated that of Bax in BMOL cells, but these effects were not observed in *Txnip* knockdown cells (Fig. 5F). In addition, the 1,25(OH)₂D₃-induced changes of PCNA, Bax, and Bcl-xL expression were blocked by pre-treatment with *Vdr* siRNA (Fig. S10).

Next, we explored whether the increased proliferation and decreased apoptosis in *Txnip*-deficient cholangiocytes contributes to the increase of ductular reaction in vivo and found that pan-CK⁺BrdU⁺ cells were significantly more numerous while pan-CK⁺caspase-3⁺ cells were significantly less numerous in DDC-fed *Txnip*^{ΔSox9} mice compared to DDC-fed *Txnip*^{fl/fl} mice (Fig. 5G). Cholangiocytes isolated from DDC-fed *Txnip*^{ΔSox9} mice further showed upregulation of *Pcna* and *Bcl2* and downregulation of *Bax*, *Casp3*, and caspase-9 (*Casp9*), compared to those isolated from DDC-fed *Txnip*^{fl/fl} mice (Fig. 5H). These results indicate that *Txnip* deficiency promotes ductular reaction by enhancing proliferation and suppressing apoptosis of cholangiocytes.

Biliary *Txnip* deficiency promotes cholangiocyte secretion of pro-inflammatory and pro-fibrogenic mediators to activate KCs and HSCs

We next investigated the mechanism by which biliary TXNIP deficiency elicited ductular reaction and promoted liver inflammation and fibrosis. In ductular reaction, reactive cholangiocytes secrete pro-inflammatory and pro-fibrogenic mediators such as TNF-α, IL-1β, IL-6, MCP-1, and TGF-β¹⁻⁷. Thus, we postulated that TXNIP might regulate this secretion to activate liver immune cells and HSCs. Notably, F4/80⁺ liver macrophages and alpha-smooth muscle actin (α-SMA)⁺ HSCs were located adjacent to pan-CK⁺ cells around portal regions and in parenchymal regions (Fig. 6A), suggesting that these cells may engage in cross-talk. To evaluate whether biliary TXNIP-regulated pro-inflammatory mediators stimulate liver immune cells and inflammatory responses, we isolated mouse primary KCs (resident liver macrophages) and co-cultured them with *Txnip*-knockdown BMOL cells. The mRNA levels of *Tnf*, *Il6*, *Il1b*, and *Ccl2* were significantly elevated in KCs co-cultured with *Txnip*-knockdown cells compared to vector control BMOL cells (Fig. 6B). *Tnf*, *Il6*, and *Ccl2* were also upregulated in *Txnip*-

knockdown BMOL cells themselves (Fig. 6C). To validate our in vitro findings, we compared cholangiocytes from DDC-fed *Txnip*^{ΔSox9} mice and DDC-fed *Txnip*^{fl/fl} mice. Our results revealed that *Tnf* was upregulated in cholangiocytes of DDC-fed *Txnip*^{ΔSox9} mice compared to DDC-fed *Txnip*^{fl/fl} mice, whereas there was no difference in the levels of *Il6*, *Il1b*, or *Ccl2* (Fig. 6D). Culture media from *Txnip*-knockdown BMOL cells contained increased levels of TNF-α (Figure S11A) and neutralization of TNF-α in the culture medium downregulated the mRNA levels of *Tnf*, *Il6*, *Il1b*, *Ccl2*, and *Adgre1* in KCs co-cultured with *Txnip*-knockdown BMOL cells (Fig. 6E, F).

To further determine how TXNIP in ductular reactive cells regulates the pro-fibrogenic potential of HSCs, in vitro co-culture assays were performed using mouse primary HSCs and *Txnip*-knockdown BMOL cells. HSCs co-cultured with *Txnip*-knockdown BMOL cells showed increased levels of *Tgfb1*, *Col1a1*, *Col3a1*, *Col4a1*, and *Mmp9* compared to HSCs co-cultured with vector control BMOL cells (Fig. 6G). qPCR analysis also showed that *Tgfb1* was upregulated in *Txnip*-knockdown BMOL cells (Fig. 6H) and in cholangiocytes isolated from DDC-fed *Txnip*^{ΔSox9} mice relative to those from DDC-fed *Txnip*^{fl/fl} mice (Fig. 6I and Fig. S11B). We next assessed whether the increased TGF-β secretion by ductular reactive cells under *Txnip* deficiency contributes to HSC activation and collagen deposition. Indeed, TGF-β levels were significantly increased in conditioned media of *Txnip*-knockdown BMOL cells (Fig. S11C) and neutralization of TGF-β in the culture medium downregulated *Col1a1*, *Col3a1*, and *Col4a1* in HSCs co-cultured with *Txnip*-knockdown BMOL cells (Fig. 6J, K). Collectively, these results suggest that *Txnip* deficiency increases the secretion of TNF-α and TGF-β in ductular reactive cells to activate neighboring KCs and HSCs and thereby promote inflammatory responses and collagen synthesis.

Protective effects of vitamin D on ductular reaction and liver inflammation and fibrosis are partially dependent on biliary TXNIP

We next evaluated whether TXNIP is required for the hepatoprotective function of vitamin D. The DDC-induced increases in pan-CK⁺BrdU⁺ and F4/80⁺ cell numbers and the mRNA upregulations of *Tnf* and *Adgre1* were significantly attenuated by 1,25(OH)₂D₃ treatment of *Txnip*^{fl/fl} mice but not *Txnip*^{ΔSox9} mice (Fig. 7A, B). 1,25(OH)₂D₃ partially reduced the Sirius red-positive area and hepatic level of *Col3a1* and *Col4a1* in both *Txnip*^{fl/fl} and *Txnip*^{ΔSox9} mice, but the mRNA expression of *Col1a1* was decreased in 1,25(OH)₂D₃-treated *Txnip*^{fl/fl} mice but not in *Txnip*^{ΔSox9} mice (Fig. 7A, C). We further examined whether the VDR-dependent induction of TXNIP in cholangiocytes is the main mechanism by which vitamin D supplementation suppresses DDC-induced ductular reaction and CLDs. To enable genetic knockdown of *Vdr* and *Txnip* in mouse cholangiocytes, adeno-associated virus 8 (AAV8)-Sox9-sh*Vdr* or AAV8-Sox9-sh*Txnip* was injected via the tail vein and then fed the mice DDC diet for 4 weeks with 1,25(OH)₂D₃ (Fig. S12A). The targeted knockdown efficiency of the adenoviral vector was confirmed by double immunofluorescence staining for pan-CK/VDR or pan-CK/TXNIP (Fig. S12B). We found that DDC diet-induced ductular reaction and hepatic inflammation and fibrosis were significantly elevated in both AAV8-Sox9-sh*Vdr* and AAV8-Sox9-sh*Txnip* injected mice compared with AAV8-Sox9-control injected mice (Fig. S13). Furthermore, 1,25(OH)₂D₃ treatment reduced DDC diet-induced ductular reaction and hepatic inflammation and fibrosis, but the effects of vitamin D supplementation on ductular reaction and inflammation were abolished in both AAV8-Sox9-sh*Vdr* and AAV8-Sox9-sh*Txnip* injected mice (Fig. S13).

To further determine the direct role of TXNIP in ductular reaction and liver inflammation and fibrosis, DDC-fed mice were given the TXNIP agonist, vorinostat. This pan-histone deacetylase inhibitor elevates TXNIP expression through direct effects on histone H4 acetylation near the TXNIP transcription start site³⁶. Here, vorinostat

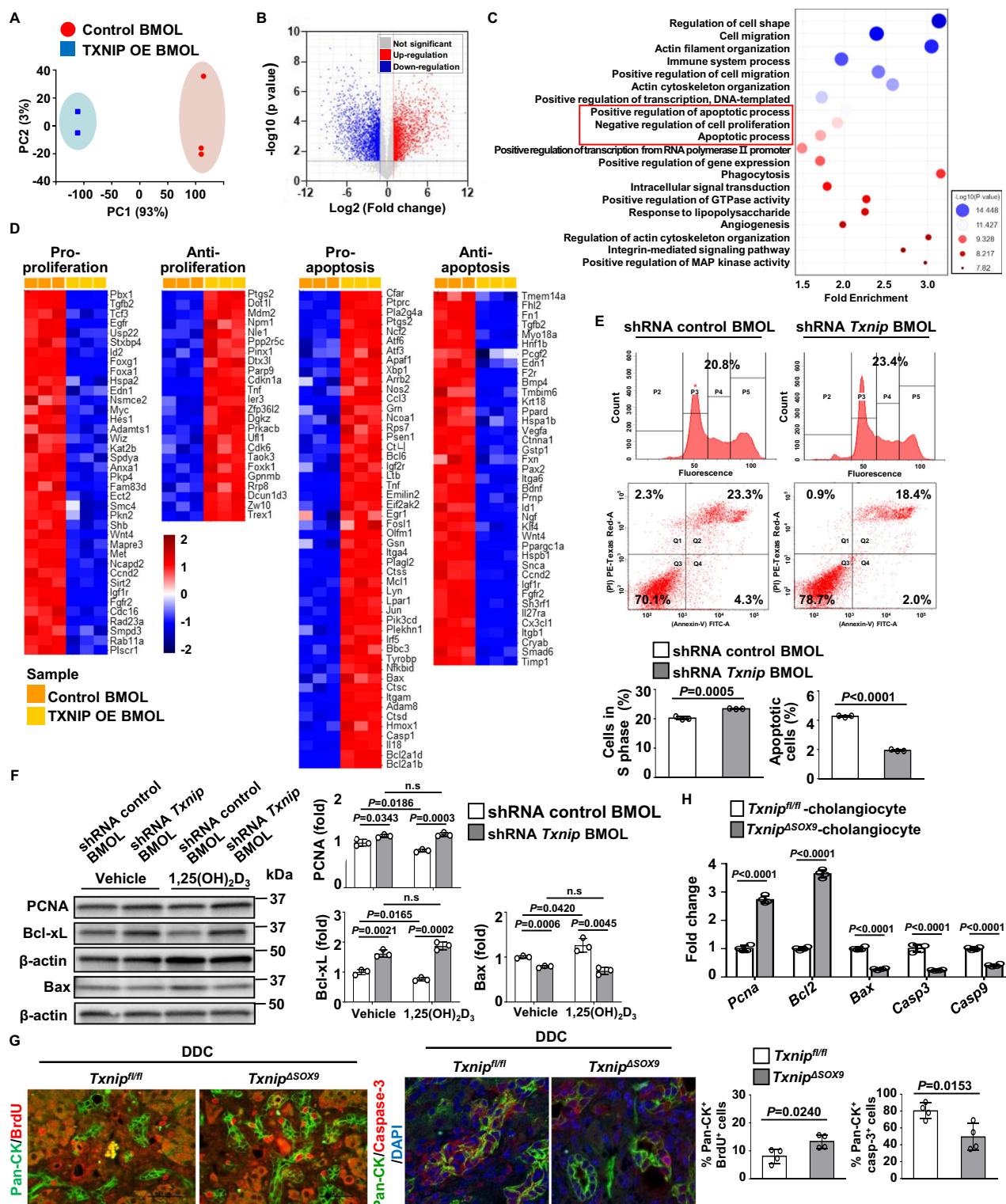


Fig. 5 | TXNIP regulates cholangiocyte proliferation and apoptosis. Principal component analysis (A) and volcano map (B) for control and *Txnip*-overexpressing (OE) BMOL cells ($n = 3$ /group). C Top 20 enriched gene ontologies from DAVID analysis. D Heatmap of representative differentially expressed genes in control and *Txnip* OE BMOL cells. E Flow cytometric analysis of shRNA control and shRNA *Txnip* BMOL cells ($n = 3$ biological replicates). F Effects of 1,25(OH)₂D₃ on cell proliferation and apoptosis in shRNA control and shRNA *Txnip* BMOL cells, as assessed by

Western blot analysis ($n = 3$ biological replicates). G IF staining of pan-CK/BrdU and pan-CK/caspase-3 in liver tissues. *Txnip*^{fl/fl} and *Txnip*^{ΔSOX9} mice were DDC-fed for 4 weeks. Right: Percentages of pan-CK⁺BrdU⁺ and pan-CK⁺caspase-3⁺ cells ($n = 4$ /group). Original magnifications: 400X and 800X. (H) qPCR analysis of cholangiocytes isolated from DDC-fed *Txnip*^{fl/fl} and *Txnip*^{ΔSOX9} mice ($n = 4$ /group). Values represent means \pm SDs. n.s., not significant. Significance determined by unpaired two-tailed *t* test. Source data are provided as a Source Data file.

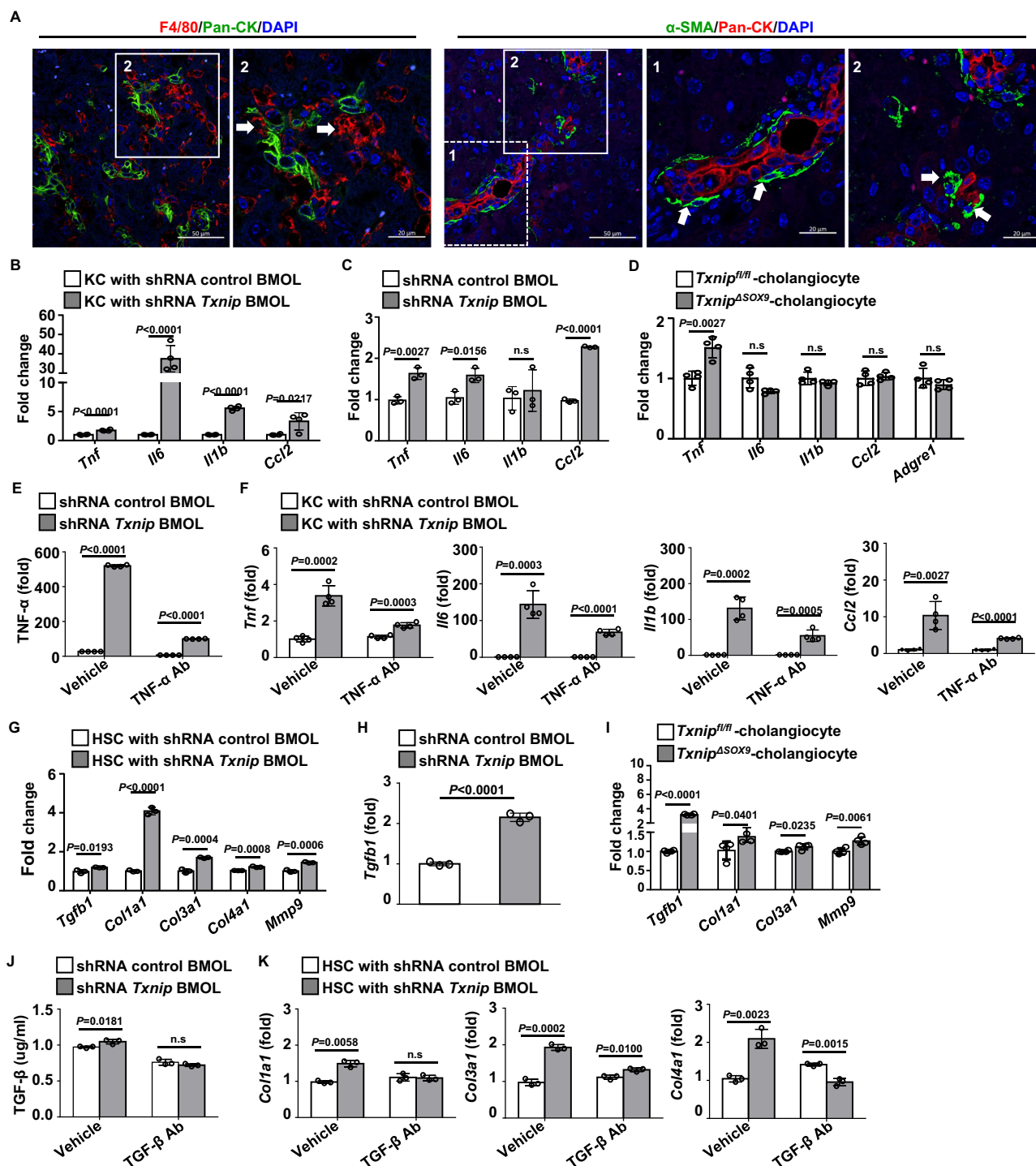


Fig. 6 | Biliary TXNIP regulates secretion of pro-inflammatory and pro-fibrogenic mediators. **A** Representative images of IF staining for F4/80/pan-CK and α-SMA/pan-CK in DDC-fed mice. F4/80⁺ liver macrophages and α-SMA⁺ HSCs were observed near pan-CK⁺ cells (arrows) near portal regions (1) and in parenchymal regions (2). Original magnifications: 400X and 800X. **B** qPCR analysis. Primary KCs isolated from C57BL/6 mice were co-cultured with shRNA control or shRNA *Txnip* BMOL cells for 24 h ($n = 4$ biological replicates). **C** mRNA levels of cytokines in shRNA control and shRNA *Txnip* BMOL cells ($n = 3$ biological replicates). **D** Relative mRNA expression levels of pro-inflammatory genes in cholangiocytes isolated from DDC-fed *Txnip*^{fl/fl} and *Txnip*^{ASOX9} mice ($n = 4$ /group). **E** Levels of TNF-α in culture media of shRNA control or shRNA *Txnip* BMOL cells treated with or without TNF-α neutralizing antibody (5 μg/ml) for 24 h ($n = 4$ biological replicates). **F** Expression of pro-inflammatory genes in KCs isolated from C57BL/6 mice and co-cultured with shRNA control or shRNA *Txnip* BMOL cells plus

TNF-α neutralizing antibody ($n = 4$ biological replicates). **G** Relative mRNA expression levels of fibrosis-related genes. HSCs isolated from C57BL/6 mice were co-cultured with shRNA control or shRNA *Txnip* BMOL cells ($n = 3$ biological replicates). **H** Relative mRNA expression levels of *Tgfb1* in shRNA control and shRNA *Txnip* BMOL cells ($n = 3$ biological replicates). **I** qPCR analysis of fibrosis-related genes in cholangiocytes from DDC-fed *Txnip*^{fl/fl} and *Txnip*^{ASOX9} mice ($n = 4$ /group). **J** Levels of TGF-β in culture media from shRNA control or shRNA *Txnip* BMOL cells treated with or without TGF-β neutralizing antibody (2 μg/ml) for 24 hours ($n = 3$ biological replicates). **K** Expression of fibrosis-related genes in primary HSCs co-cultured with shRNA control or shRNA *Txnip* BMOL cells with or without TGF-β neutralizing antibody ($n = 3$ biological replicates). Values represent means ± SDs. n.s., not significant. Significance determined by unpaired two-tailed *t* test. Source data are provided as a Source Data file.

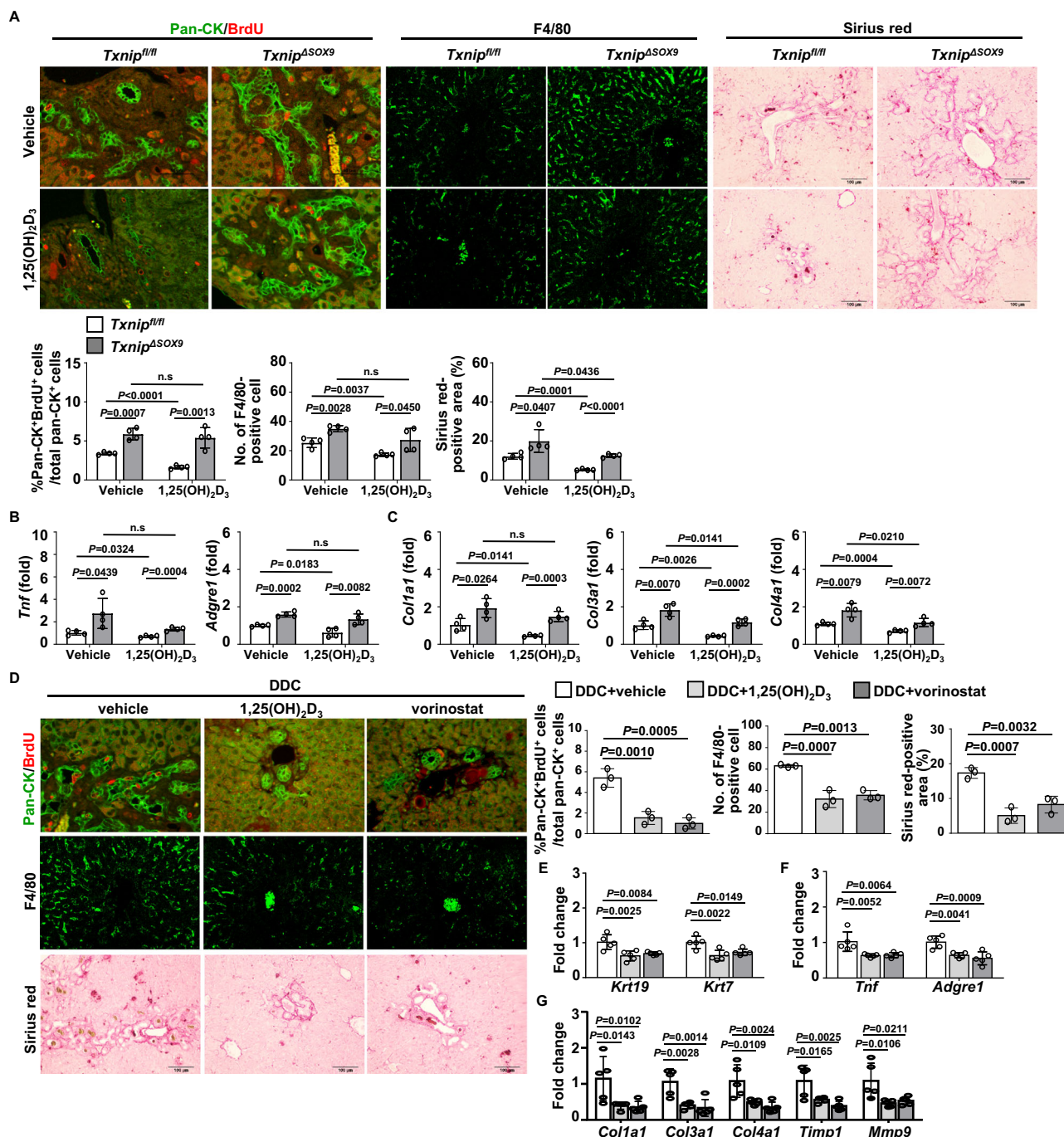


Fig. 7 | Vitamin D attenuates DDC-induced ductular reaction and liver inflammation and fibrosis via TXNIP. Female *Txnip^{fl/fl}* and *Txnip^{ASOX9}* mice were fed DDC diet with 1,25(OH)₂D₃ (5 µg/kg, 2x week). Shown are representative images of IF staining for pan-CK/BrdU and F4/80, and Sirius-red staining (A), hepatic expressions of pro-inflammatory genes (B), and relative mRNA levels of collagen in liver (C) ($n=4$ /group). Lower: Percentages of pan-CK⁺BrdU⁺ cells, F4/80⁺ cells, and Sirius red-positive areas. Original magnification: 200X and 400X. D–G Female C57BL/6 mice

were fed DDC diet with 1,25(OH)₂D₃ or vorinostat (100 mg/kg, 2x week). Shown are: IF staining of pan-CK/BrdU and F4/80, and Sirius-red staining (D) ($n=3$ /group), and expression levels of genes involved in ductular reaction (E), inflammatory cytokines (F), and fibrosis (G) ($n=5$ /group). Original magnification: 200X and 400X. Values represent means \pm SDs. n.s., not significant. Significance determined by unpaired two-tailed *t* test (A, B, C) and one-way ANOVA followed by Tukey's multiple comparisons test (D, E, F, G). Source data are provided as a Source Data file.

treatment dose-dependently increased *Txnip* expression in BMOL cells (Fig. S14). Compared with vehicle-treated mice, vorinostat-treated mice exhibited significant decreases in the pan-CK⁺BrdU⁺ cell number and *Ck19* and *Ck7* expression levels, which were comparable to those seen in 1,25(OH)₂D₃-treated mice (Fig. 7D, E). Vorinostat administration also decreased the numbers of F4/80⁺ cells, and Sirius red-positive areas, and downregulated *Tnf*, *Adgre1*, *Col1a1*, *Col3a1*, *Col4a1*, *Timp1*, and *Mmp9* (Fig. 7D, F, G). To evaluate whether vorinostat has the same

effect as vitamin D on liver cells, we isolated cholangiocytes, HSCs, and liver macrophages from mice given standard rodent chow diet plus vehicle, DDC plus vehicle, and DDC plus vorinostat. Similar to the results obtained with vitamin D treatment, the DDC diet feeding-induced upregulations of *Pcna* and *Tnf* were significantly reduced, whereas *Casp3* was increased, in cholangiocytes from vorinostat-treated mice (Fig. S15). In addition, the expression levels of *Acta2*, *Col1a1*, *Col3a1*, and *Col4a1* in HSCs and those of *Tnf*, *Il1b* and *Ccl2* in

liver macrophages were downregulated in vorinostat-treated mice (Fig. S15). Together, these findings indicate that the vitamin D-induced upregulation of TXNIP could potentially be developed to therapeutically address ductular reaction and CLD.

In patients with CLDs, TXNIP expression in ductular reaction cells positively correlates with vitamin D plasma levels

We previously reported that TXNIP expression is upregulated in patients with ALD and MASLD^{28,29}. Here, we evaluated the expression levels of TXNIP in patients with CLDs. TXNIP was expressed as follows: in hepatocytes and LSECs of normal individuals, with increased expression in CLD patients; in cholangiocytes and HSCs of normal individuals, with weak or absent expression in CLD patients; and in liver macrophages, at similar levels in normal individuals and CLD patients (Fig. S16).

We further investigated the clinical significance of the vitamin D/TXNIP axis in ductular reaction and liver inflammation and fibrosis. We found that Pan-CK⁺ and SOX9⁺ cells strongly co-expressed TXNIP in biliary epithelial cells of control individuals (Fig. 8A). In patients with CLDs, in contrast, pan-CK⁺ and SOX9⁺ cells that were detached from the bile duct structure and penetrated into the surrounding matrix showed no TXNIP staining (Fig. 8A). Far fewer TXNIP⁺pan-CK⁺ and TXNIP⁺SOX9⁺ cells were observed in patients with CLDs compared to control individuals (Fig. 8B, C). The numbers of TXNIP⁺pan-CK⁺ and TXNIP⁺SOX9⁺ cells were negatively correlated with hepatic biochemical parameters, and patients with more advanced (stage 4) fibrosis had fewer TXNIP⁺pan-CK⁺ and TXNIP⁺SOX9⁺ cells (Fig. 8D and Figure S17). Finally, TXNIP expression in ductular reactive cells was positively correlated with the vitamin D plasma level (Fig. 8E).

In line with the findings in humans, TXNIP⁺pan-CK⁺ and TXNIP⁺SOX9⁺ cell numbers were markedly decreased in DDC-fed mice compared to chow diet-fed mice (Fig. S18A, B) and TXNIP expression in ductular reactive cells was negatively correlated with the F4/80⁺ cell number and Sirius red-positive area (Fig. S18C, D). BDL mice also showed lower TXNIP⁺pan-CK⁺ and TXNIP⁺SOX9⁺ cell numbers than sham mice, and exhibited negative relationships between the TXNIP level and the F4/80⁺ cell number and Sirius red-positive area (Figure S19).

Discussion

Vitamin D deficiency is associated with CLDs regardless of etiology³⁷, but the mechanisms through which vitamin D supplementation may regulate CLD progression remain largely unknown. The current study revealed that vitamin D plasma levels are decreased in patients with CLDs and negatively correlated with ductular reaction severity. In DDC-fed and BDL mice, 1,25(OH)₂D₃ treatment reduced ductular reaction and liver inflammation and fibrosis, and significantly upregulated TXNIP in ductular epithelial cells. This elevated TXNIP inhibited cholangiocyte proliferation while increasing cholangiocyte death to ameliorate the ductular reaction. TXNIP also decreased the secretions of TNF- α and TGF- β by ductular reactive cells; this inhibited the activations of KCs and HSCs to prevent inflammatory responses and collagen deposition. In patients with CLDs, biliary TXNIP expression was profoundly downregulated and positively correlated with vitamin D plasma levels, suggesting that a similar vitamin D/TXNIP cascade may be relevant to human liver diseases. Our findings provide mechanistic insights into the protective effects of vitamin D supplementation in ductular reaction and CLDs, as summarized in the working model presented in Fig. 8F.

Although ductular reaction is common to almost all CLDs and ductular reactive cells represent a cell type crucial for liver function and architecture, there is little data on their proliferation and interaction with other cell populations in liver disease. We thus lack therapeutic strategies targeting ductular reaction. Here, we found that vitamin D plasma levels in patients with CLDs were negatively correlated with the degree of ductular reaction, and vitamin D supplementation ameliorated DDC-induced cholangiocyte proliferation and ductular reaction in mice. We further observed the following: vitamin

D upregulated TXNIP expression in cholangiocytes; *Txnip* deletion in cholangiocytes abolished the protective effects of vitamin D; and direct agonist-induced TXNIP overexpression attenuated the DDC-induced ductular reaction. Together, our findings indicate that these protective functions of vitamin D are mediated by the upregulation of TXNIP. Previous studies showed that vitamin D restrains cell proliferation and induces differentiation and apoptosis in various normal and tumor cells. For example, in HPCs, vitamin D reportedly suppressed cell proliferation, invasion, and dedifferentiation³⁸. TXNIP induced G1 cell cycle arrest in HCC cells by stabilizing p27kip1³⁹, while loss of TXNIP promoted hepatocyte proliferation via TNF- α /NF- κ B activation^{40,41}. TXNIP expression is low in human HCC, and vitamin D treatment of HCC cells stimulated TXNIP transcription to inhibit proliferation and promote apoptosis²⁶. The present study explores the vitamin D/TXNIP axis in ductular reaction and CLDs. Our findings indicate that vitamin D supplementation-triggered TXNIP overexpression critically modulates ductular reaction by regulating cholangiocyte proliferation and apoptosis.

How does vitamin D regulate TXNIP expression? Previously, vitamin D was reported to exert a wide range of biological actions through the nuclear VDR-mediated transcriptional regulation of target genes⁴². Here, we observed that VDR knockdown in cholangiocytes abolished the hepatoprotective effects of 1,25(OH)₂D₃ in DDC diet-fed mice. More importantly, the 1,25(OH)₂D₃-induced TXNIP upregulation was significantly blocked by VDR silencing, and a luciferase reporter gene assay showed that vitamin D enhanced *Txnip* promoter activity via VDR. This is in line with several previous reports highlighting the crucial role of VDR in cholangiocytes and liver disease development. VDR activation was reported to attenuate BDL-induced liver injury by promoting bile duct repair through Yes-associated protein (YAP) upregulation⁴³, whereas VDR knockout exacerbated cholestatic liver injury and diminished bile duct integrity through the epidermal growth factor receptor (EGFR) pathway⁴⁴. Based on our observations, we postulate that the hepatoprotective effects of vitamin D supplementation in liver diseases are mainly driven by the VDR-dependent induction of TXNIP in cholangiocytes.

Although this study suggests that the vitamin D/VDR/TXNIP axis could directly regulate ductular reaction via cholangiocytes, vitamin D can also impact other liver cell types via VDR. In particular, we found that vitamin D treatment significantly reduced the DDC diet-induced activations of HSCs and liver macrophages, and these cells showed upregulation of VDR. This suggests that the vitamin D-induced and VDR-mediated inactivation of HSCs and liver macrophages can indirectly inhibit ductular reaction. This hypothesis is supported by studies showing that activated HSCs could upregulate the Notch and Hedgehog pathway in HPCs to facilitate HPC differentiation into biliary cells and bile duct formation^{7,45,46}. Previous reports also showed that macrophages are increased significantly in the ductular reaction area, and this is related to the expansion of CK7⁺ HPCs^{46–48}. Here, we found that 1,25(OH)₂D₃ treatment upregulated the expression levels of VDR and TXNIP mainly in cholangiocytes and biliary *Vdr* or *Txnip* knockdown in mice abolished the hepatoprotective function of vitamin D. Together, these findings indicate that the effects of vitamin D on ductular reaction occur mainly through cholangiocytes in our model, although HSCs and liver macrophages may indirectly regulate ductular reaction.

Proliferating cholangiocytes secrete various pro-inflammatory and profibrotic cytokines that undergo cross-talk with other cells in the hepatic microenvironment^{4–7}. Here, we found that conditioned media of *Txnip*-knockdown BMOL cells exhibited increased accumulation of TNF- α and TGF- β . Pro-inflammatory cytokines and profibrotic genes were significantly increased in KCs and HSCs, respectively, stimulated with conditioned media of *Txnip*-knockdown BMOL cells. The key role of TXNIP in regulating cholangiocytes is emphasized by our observation that TNF- α and TGF- β expression levels were upregulated in primary cholangiocytes isolated from DDC-fed *Txnip*^{ΔSOX9} mice. These

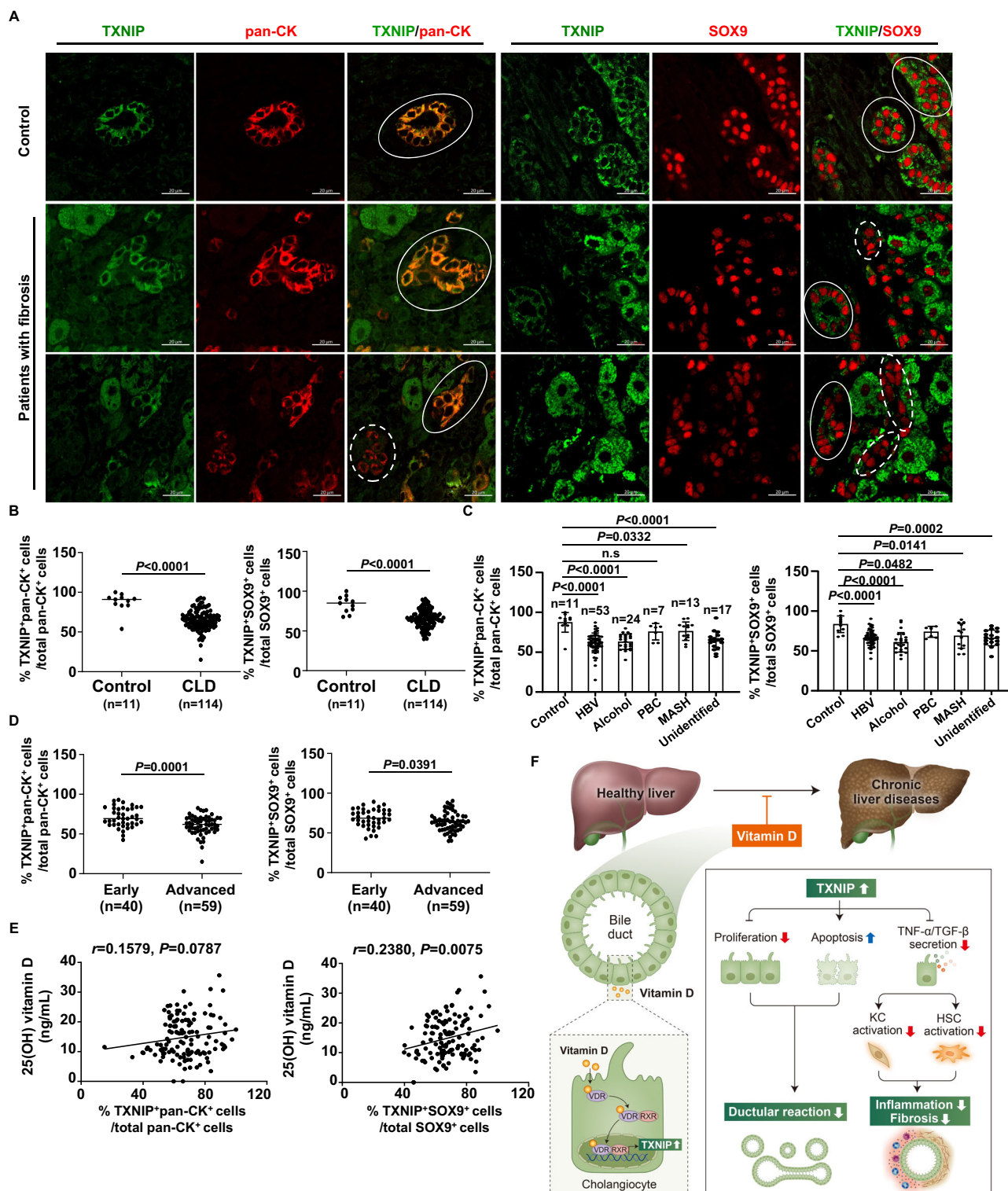


Fig. 8 | Correlation between biliary TXNIP expression and vitamin D levels in patients with CLDs. **A** Representative images of IF staining for TXNIP/pan-CK (left) and TXNIP/SOX9 (right) in liver sections from control individuals and patients with CLDs. White circles indicate TXNIP⁺ cholangiocytes; open circles show decrease or loss of TXNIP expression in cholangiocytes. Original magnification: 800X.

B Percentages of TXNIP⁺pan-CK⁺ and TXNIP⁺SOX9⁺ cells (controls, $n = 11$; patients with CLDs, $n = 114$). **C** Percentages of TXNIP⁺pan-CK⁺ and TXNIP⁺SOX9⁺ cells in controls ($n = 11$) and patients with CLDs categorized by etiology, including HBV ($n = 53$), alcohol ($n = 24$), PBC ($n = 7$), MASH ($n = 13$), and unidentified ($n = 17$).

D Percentages of TXNIP⁺pan-CK⁺ and TXNIP⁺SOX9⁺ cells in early ($n = 40$) and

advanced ($n = 59$) fibrosis. **E** Association between TXNIP expression in cholangiocytes and vitamin D levels ($n = 125$). **F** Proposed mechanisms by which vitamin D may exert hepatoprotection against CLDs. Vitamin D induces TXNIP expression in ductular epithelial cells via VDR. The elevated TXNIP inhibits cholangiocyte proliferation while increasing cholangiocyte death, ameliorating ductular reaction. TXNIP also downregulates TNF- α and TGF- β secretion by ductular reactive cells, inhibiting KC and HSC activation to prevent inflammation and fibrosis. Values represent means \pm SDs. Significance determined by unpaired two-tailed t test (**B**, **C**, **D**). Correlations were assessed by Pearson correlation coefficient and line of best-fit was generated by simple linear regression analysis (**E**). Source data are provided as a Source Data file.

findings suggest that the loss of *Txnip* in cholangiocytes potentially stimulates TNF- α and TGF- β secretion to activate KCs and HSCs through paracrine actions and thereby promote liver inflammation and fibrosis. This hypothesis is further supported by our observation that neutralization of TNF- α or TGF- β in conditioned media of *Txnip*-knock-down BMOL cells decreased the activation of co-cultured KCs and HSCs. Similarly, TXNIP deficiency was reported to upregulate TNF- α in hepatocytes and enhance TGF- β -mediated transcriptional activity in a cancer cell line^{41,49}. Although further studies are needed to determine how TXNIP regulates TNF- α and TGF- β in cholangiocytes, our results indicate that, upon upregulation via vitamin D/VDR, biliary TXNIP directly inhibits TNF- α and TGF- β to block the paracrine activation of KCs and HSCs and thereby prevent liver disease progression.

Despite the advances described herein, this study has several limitations and some questions remain unanswered. First, although the vitamin D level did not differ between early and advanced fibrosis patients, these patient groups exhibited significant differences in ductular reaction markers. We therefore examined the correlation between vitamin D level and ductular reaction depending on the etiology. Patients with HBV and alcohol exhibited a negative relationship between the vitamin D level and ductular reaction (severity assessed using the number of pan-CK⁺ or SOX9⁺ cells), whereas this correlation was low in patients with PBC and MASH. These results indicate that the negative correlation observed in the overall population between vitamin D level and ductular reaction markers was mainly due to patients with CLD etiologies related to HBV and alcohol. However, the low correlation seen in the PBC and MASH groups may also reflect that our study included relatively few such patients ($n = 7$ and 13 , respectively). Further study with larger patient groups will be needed to evaluate whether PBC and MASH patients show a negative correlation between their vitamin D level and ductular reaction. Second, vitamin D has been reported to exert anti-fibrotic effects on HSCs via its interaction with VDR^{31,33,34}, suggesting a potential physiologic role for vitamin D/VDR-mediated liver fibrosis. In HSCs, VDR signaling activation was shown to antagonize multiple TGF- β /SMAD-dependent transcriptional changes in profibrotic genes³³. Here, we found that vitamin D treatment did not affect DDC-induced ductular reaction in *Txnip*^{ΔSox9} mice, but partially reduced DDC-induced liver fibrosis in these mice. This may reflect that vitamin D acts directly on HSCs via VDR in *Txnip*^{ΔSox9} mice. We observed that TXNIP was localized both in HSCs and cholangiocytes of normal individuals, but the expression level was decreased in CLD patients. The expression levels of TXNIP and VDR were upregulated in HSCs from vitamin D-treated mice, suggesting that vitamin D-induced VDR/TXNIP upregulation in HSCs could directly regulate liver fibrosis. It could be very useful to generate an HSC-specific *Txnip* knockout mouse strain and use it to explore the roles of the vitamin D/VDR/TXNIP axis in HSC activation and liver fibrosis.

Accumulating data indicate that vitamin D affects the progression of CLDs at several stages, such as by inhibiting the injury trigger, suppressing liver macrophages and HSC activation and proliferation, reducing cytokine levels and ECM accumulation, and degrading collagen through MMP activation and TIMP inhibition^{18–21}. Here, we report on how vitamin D supplementation impacts the ductular reaction and subsequent progression of liver inflammation and fibrosis. Our pre-clinical data reveal a new mechanism by which vitamin D supplementation ameliorates CLDs and support the idea that the vitamin D/TXNIP axis could be a promising therapeutic target in clinically addressing the ductular reaction and CLDs.

Methods

Ethical statement

This study was conducted in strict accordance with all relevant ethical regulations and animal welfare legislation in Korea. The study conformed to the ethical principles for medical research involving human subjects outlined in the 2013 Declaration of Helsinki and abided by the

2018 Declaration of Istanbul. The study protocol was approved by the Institutional Review Board of Chungnam National University Hospital (IRB number: 2016-03-020-0449 and 2020-02-042-011). All animal experiments were conducted in accordance with the principles and procedures outlined in the ARRIVE (Animals in Research: Reporting In Vivo Experiments) statement and were approved by the Chungnam National University Animal Care and Use Committee (Approval Number: 202304A-CNU-069, 202409A-CNU-165, and 202410A-CNU-187). Previous studies showed that female mice exhibit increased ductular reaction compared with male mice, due to the higher activity of the hepatic cytochrome P450 (CYP), the enzyme responsible for DDC metabolism^{50,51}. We used only female mice to induce more severe ductular reaction. Mice were housed under a 12-hour light–dark cycle, with five mice per cage. The ambient temperature was maintained at 21 ± 1 °C, with a humidity level of $50 \pm 10\%$.

Human liver samples

Human plasma samples and liver tissues were obtained from patients with CLDs ($n = 114$) of various etiologies (HBV, $n = 53$; alcohol, $n = 24$; PBC, $n = 7$; MASH, $n = 13$; unidentified, $n = 17$) and control ($n = 11$). The CLD cohort included patients at fibrosis stage 1 ($n = 24$), fibrosis stage 2 ($n = 16$), fibrosis stage 3 ($n = 15$), and fibrosis stage 4 ($n = 59$). Plasma samples and liver tissues from control individuals were collected from donors whose livers were prepared for liver transplantation. We obtained informed consent from all participants not only for participation in the study but also for the publication and dissemination of the study results. Detailed information on the patients is presented in Table S1.

Animal experiments

Txnip floxed (*Txnip*^{fl/fl}; strain #016847) and *Sox9-CreER* (strain #035092) mice were obtained from Jackson Laboratories (Bar Harbor, ME, USA). Cholangiocyte-specific *Txnip*-deficient (*Txnip*^{fl/fl}*Sox9-CreER*⁺; *Txnip*^{ΔSox9}) mice were generated by crossing *Txnip*^{fl/fl} mice with *Sox9-CreER* mice on a C57BL/6 background. Cre-negative *Txnip*^{fl/fl} (*Txnip*^{fl/fl}*Sox9-CreER*[−]; *Txnip*^{fl/fl}) mice were used as littermate controls. Tamoxifen-mediated induction of Cre activity was performed in 4- to 6-week-old mice by daily intraperitoneal injection of 75 mg tamoxifen (Sigma-Aldrich, St. Louis, MO, USA)/kg body weight for 5 consecutive days. Two weeks after the last injection of tamoxifen, the absence of *Txnip* in cholangiocytes was verified by immunofluorescence (IF) and qPCR analyses. For acute deletion of *Vdr* and *Txnip* in cholangiocytes, female C57BL/6 mice were given two doses of AAV8-*Sox9*-control, AAV8-*Sox9*-sh*Vdr*, or AAV8-*Sox9*-sh*Txnip* (1×10^{11} GC/mouse, i.v.; GeneChem, Shanghai, China). Here, eight-week-old female mice were fed a standard rodent chow diet or DDC diet (Research Diets, Inc., NJ, USA) for 10 days, 4 weeks, or 12 weeks. For vitamin D and TXNIP agonist treatments, 1,25(OH)₂D₃ (5 μg/kg, 2x week; MedChemExpress, Monmouth Junction, NJ, USA) and vorinostat (100 mg/kg, 2x week; MedChemExpress) were injected intraperitoneally during the 4-week period mice were fed with the standard or DDC diet. To explore a second model of ductular reaction, mice were given BDL or sham surgery and treated with 1,25(OH)₂D₃ (5 μg/kg, 2x week; MedChemExpress). Age (8 weeks)- and sex-matched littermates were used for experiments.

Histological examination

Formalin-fixed liver samples were paraffin embedded, sectioned at 4 μm, and stained with H&E (Labcore, Seoul, Korea). For examination of collagen deposition in liver tissues, paraffin sections were stained with Sirius red (IHC World, Woodstock, MD, USA), counterstained with Mayer's hematoxylin, and analyzed via light microscopy. For Sirius red-positive area quantification, portal area around region were selected and the positive area was calculated from at least five magnification (200X) fields per liver section using the ImageJ software (1.53k; National Institutes of Health, Rockville, MD, USA).

Immunohistochemistry (IHC) analysis

Paraffin-embedded liver tissues from human and mice were blocked with 10% normal goat serum (Vector Laboratories, Newark, CA, USA) and incubated with primary antibodies against pan-CK (Bioss, Woburn, MA, USA), SOX9 (Abcam, Cambridge, UK), and F4/80 (Abcam) (Table S2). The slides were counterstained with Mayer's hematoxylin, dehydrated, and mounted with mounting medium (Mercedes Scientific, Lakewood Ranch, FL, USA). To analyze ductular reaction, five fields were randomly selected from each slide, and all positively stained cells in each image were counted (final magnification, 400X). Representative images were taken under an Eclipse Ni-U microscope (Nikon, Tokyo, Japan) using a Digital Sight DS-Fi3 camera controller and NIS-Elements (Nikon).

Immunofluorescence (IF) analysis

Human and mouse liver sections were incubated with primary antibodies against TXNIP (Medical & Biological Laboratories, Tokyo, Japan), albumin (Novus Biologicals, Toronto, Canada), LYVE1 (R&D Systems, Minneapolis, MN, USA), CD68, SOX9 (Abcam), pan-CK (Abcam), caspase-3 (Cell Signaling Technology, Danvers, MA, USA), TGF- β 1 (Santa Cruz Biotechnology, Dallas, TX, USA), F4/80 (Abcam), or α -SMA (Sigma-Aldrich, St. Louis, MO, USA) (Table S2), and incubated with fluorescence-conjugated antibodies. All samples were mounted with Fluoroshield™ containing 4',6-diamidino-2-phenylindole (DAPI; Invitrogen, Waltham, MA, USA) and observed under a confocal microscope (LSM 880; Carl Zeiss, Oberkochen, Germany). For BrdU staining, a BrdU IF detection kit (Thermo Fisher Scientific, Waltham, MA, USA) was used according to the manufacturer's protocol. Single-positive and double-positive cells were counted from 10 randomly selected fields per section (final magnification, 400X).

Western blotting

Liver tissues or cell lysates were homogenized in radio-immunoprecipitation assay (RIPA) buffer (Cell Signaling Technology) supplemented with protease inhibitors (Roche, Basel, Switzerland) and phosphatase inhibitors (Roche). Proteins (10 μ g) were separated by SDS-PAGE and transferred to polyvinylidene difluoride (PVDF) membranes (Bio-Rad Laboratories, Hercules, CA, USA). The membranes were blocked with 5% bovine serum albumin (BSA) for 1 h at room temperature and then incubated with primary antibodies against TXNIP (Abcam), Bax (Santa Cruz Biotechnology), PCNA, Bcl-xL, VDR (Cell Signaling Technology), or β -actin (Sigma-Aldrich) (Table S2). Immunoreactive bands were visualized using alkaline phosphatase-conjugated anti-mouse or rabbit antibodies (Sigma-Aldrich) and the SuperSignal plus chemiluminescent substrate (Thermo Fisher Scientific). Bands were imaged using an ImageSaver6 (ATTO, Tokyo, Japan) without saturation and analyzed with the CSAnalyzer 4 software (ATTO). The band intensity was normalized to that of β -actin; all band detections were within the linear range.

qPCR

Total RNA was extracted from mouse liver tissues and cells using TRIzol (Thermo Fisher Scientific) according to the manufacturer's instructions. The corresponding cDNA was synthesized using a ReverTra Ace® qPCR RT Kit (Toyobo, Osaka, Japan). Relative gene expression levels were measured by qPCR using the SYBR Green PCR Master Mix (Applied Biosystems, Waltham, MA, USA) and a StepOne™ Real-Time PCR System (Applied Biosystems). The relative expression levels of target genes were quantified using qPCR analysis, with *gapdh* detected as an internal control. The fold change of mRNA was expressed as $2^{-\Delta\Delta Ct}$. The primer pairs used for qPCR are listed in the Table S3.

Human 25(OH) vitamin D level analysis

For the quantitative determination of 25(OH) Vitamin D in plasma from healthy control individuals and patients with fibrosis, we used a

commercial enzyme-linked immunosorbent assay kit (ALPCO Diagnostics, Salem, NH, USA) as described by the manufacturer.

In vitro experiment

BMOL cells, which represent a mouse ductular cell/hepatic progenitor cell line, were kindly provided by Dr. Yeoh (University of Western Australia, Perth, Australia) and cultured in Williams E medium supplemented with 10% FBS, 1% penicillin, and streptomycin. To establish stable cell lines with overexpressed and knockdown *Txnip*, BMOL cells were transfected with negative control construct, TXNIP-expressing construct, negative control shRNA, or *Txnip* shRNA (EX-NEG-M68, EX-Mm07552-M68, CSHCTR001-mH1, and MSN023863-mH1a, respectively; GeneCopeia, Rockville, MD, USA) using the Xfect transfection reagent (Clontech Laboratories, Mountain View, CA, USA) according to the manufacturer's protocol. Positive clones were selected with puromycin for 3 weeks and identified using qPCR and Western blotting. For *Vdr* knockdown, mouse *Vdr* siRNA or control siRNA (Dharmacon, Lafayette, CO, USA) was prepared in RNase-free suspension buffer at 5 pmol/ μ L. Cells were transfected with siRNA (final concentration, 25 pmol/mL) for 48 h and used for qPCR or Western blotting. For drug treatment, BMOL cells were incubated for 24 h in culture medium containing 1,25(OH) $_2$ D $_3$ (10 μ mol/L; MedChemExpress) with or without siRNA administration. For co-culture assays, primary HSCs or KCs (resident liver macrophages) isolated from C57BL/6 mice were seeded to 6-well plates and BMOL cells were seeded to polycarbonate membrane cell culture inserts (0.4 μ m pores; Corning, Kennebunk, ME, USA). Inserts containing BMOL cells were incubated overnight and then placed in the 6-well plates containing HSCs or KCs. For co-culture experiments, the cells were incubated for 24 h in fresh medium with or without TGF- β neutralizing antibody (final concentration, 2 μ g/mL; R&D Systems Minneapolis, MN, USA) or TNF- α neutralizing antibody (final concentration, 5 μ g/mL; R&D Systems). Thereafter, the trans-well inserts were carefully removed, supernatants were collected for further analyses, and the HSCs or KCs were immediately homogenized for RNA extraction. MMNK-1 cells, representing a human cholangiocyte cell line, were purchased from JCRB cell bank (Osaka, Japan) and cultured in Dulbecco's modified Eagle's medium (DMEM). For drug treatment, the MMNK-1 cells were treated with 1,25(OH) $_2$ D $_3$ (0.5 μ mol/L) in the culture medium for 2 h.

Primary mouse cell isolation

Primary mouse hepatocytes, HSCs, liver macrophages, and LSECs were isolated from 10-week-old female mice. Briefly, liver was perfused with collagenase, and collected non-parenchymal cells (NPCs) were separated with Opti-Prep gradients (Sigma-Aldrich) to isolate HSC and liver macrophages/LSEC fractions. Each LSEC and liver macrophages-enriched fraction was applied to the magnetic column of a magnetic-activated cell sorting (MACS) separator using anti-CD146 magnetic beads (Miltenyi Biotec, Bergisch Gladbach, Germany). Primary cholangiocytes were isolated from 10-week-old female mice. Briefly, liver was perfused with collagenase I (Sigma-Aldrich)-containing buffer and further digested with collagenase I and pronase (Roche). Collected NPCs were separated using a Percoll gradient and incubated with microbead-conjugated anti-EpCAM (Miltenyi Biotec), and EpCAM-positive cholangiocytes were purified through a MACS column (Miltenyi Biotec).

Flow cytometry

Cell populations in various phases of the cell cycle was measured using propidium iodide (PI) staining solution (Molecular Probes, Eugene, OR, USA). For apoptotic cell analysis, a FITC Annexin V Apoptosis Detection Kit (BD Pharmingen, San Diego, CA, USA) was used. All assay procedures were performed according to the manufacturers' protocols.

Immunoassay

BMOL cells were incubated with or without KCs or HSCs, and the concentrations of TNF- α and TGF- β in the conditioned media were

determined using a colorimetric assay kit (R&D Systems) according to the manufacturer's protocol. Briefly, the cell culture supernatant was loaded to a TNF- α or TGF- β antibody-coated 96-well microplate, which was incubated, washed, and decanted, and then loaded with TNF- α or TGF- β conjugate. After incubation, plate was washed, loaded with substrate solution, incubated again, and loaded with stop solution. Optical density was determined at a wavelength of 450 nm.

Luciferase-based promoter assay

A stable cell line was created by using the Xfect transfection reagent to transform BMOL cells with a luciferase-encoding vector containing control or *Txnip* promoter sequences (negative control, NEG-PG04; positive control, MPRM39646-PG4; *Txnip* promoter, MPRM30333-PG04; GeneCopeia) according to the manufacturer's protocol. Clones were selected with puromycin for 3 weeks and identified using quantitative qPCR. Luciferase activity was determined using a luciferase assay kit (GeneCopeia) according to the manufacturer's protocol. Briefly, the BMOL cells were treated for 6 h with 1,25(OH) $_2$ D $_3$, the cell culture medium was collected, and luciferase activity was measured with a luminometer and normalized to the intensity of alkaline phosphatase activity.

RNA-seq and analysis

RNA samples were collected from vector control and *Txnip*-over-expressing BMOL cells. Total RNA was isolated using the TRIzol reagent (Thermo Fisher Scientific). For control and test RNAs, library construction was performed using a QuantSeq 3' mRNA-Seq Library Prep Kit (Lexogen, Vienna, Austria) according to the manufacturer's instructions. High-throughput sequencing was performed as single-end 75 sequencing using a NextSeq 550 (Illumina, Inc., San Diego, CA, USA). DEGs were identified as having log fold change >2.0 and corrected *P* value <0.05. The mRNA-Seq data discussed herein were deposited to NCBI's Gene Expression Omnibus under GEO Series accession number GSE244700 (<https://www.ncbi.nlm.nih.gov/geo/query/acc.cgi?acc=GSE244700>).

Statistical analyses and reproducibility

Data were analyzed using GraphPad Prism (version 6; GraphPad Software, San Diego, CA, USA) and are expressed as means \pm standard deviations (SDs). Unpaired two-tailed Student's *t*-test was used to compare mean values between two groups. One-way ANOVA with post-hoc Tukey's test was used to compare data across three or more groups. The relationships between TXNIP expression and clinicopathological features were analyzed using the Chi-squared test. Spearman's correlation test was used to measure the strength of association between two variables. At least three experiments were repeated independently with similar results. *P*-value <0.05 was considered statistically significant.

Reporting summary

Further information on research design is available in the Nature Portfolio Reporting Summary linked to this article.

Data availability

The data supporting the findings from this study are available within the manuscript and its supplementary information. The datasets generated for the mRNA-Seq are available through the Gene Expression Omnibus under accession code [GSE244700](https://www.ncbi.nlm.nih.gov/geo/query/acc.cgi?acc=GSE244700). Source data are provided with this paper.

References

- Lowes, K. N., Brennan, B. A., Yeoh, G. C. & Olynyk, J. K. Oval cell numbers in human chronic liver diseases are directly related to disease severity. *Am. J. Pathol.* **154**, 537–541 (1999).
- Gouw, A. S., Clouston, A. D. & Theise, N. D. Ductular reactions in human liver: diversity at the interface. *Hepatology* **54**, 1853–1863 (2011).
- Sato, K. et al. Ductular Reaction in Liver Diseases: Pathological Mechanisms and Translational Significances. *Hepatology* **69**, 420–430 (2019).
- Zhang, Z. et al. Biliary NIK promotes ductular reaction and liver injury and fibrosis in mice. *Nat. Commun.* **13**, 5111 (2022).
- Arino, S. et al. Ductular reaction-associated neutrophils promote biliary epithelium proliferation in chronic liver disease. *J. Hepatol.* **79**, 1025–1036 (2023).
- Aguilar-Bravo, B. et al. Ductular Reaction Cells Display an Inflammatory Profile and Recruit Neutrophils in Alcoholic Hepatitis. *Hepatology* **69**, 2180–2195 (2019).
- Williams, M. J., Clouston, A. D. & Forbes, S. J. Links between hepatic fibrosis, ductular reaction, and progenitor cell expansion. *Gastroenterology* **146**, 349–356 (2014).
- Clouston, A. D. et al. Fibrosis correlates with a ductular reaction in hepatitis C: roles of impaired replication, progenitor cells and steatosis. *Hepatology* **41**, 809–818 (2005).
- Richardson, M. M. et al. Progressive fibrosis in nonalcoholic steatohepatitis: association with altered regeneration and a ductular reaction. *Gastroenterology* **133**, 80–90 (2007).
- Sancho-Bru, P. et al. Liver progenitor cell markers correlate with liver damage and predict short-term mortality in patients with alcoholic hepatitis. *Hepatology* **55**, 1931–1941 (2012).
- Feldman, D., Krishnan, A. V., Swami, S., Giovannucci, E. & Feldman, B. J. The role of vitamin D in reducing cancer risk and progression. *Nat. Rev. Cancer* **14**, 342–357 (2014).
- Rosen, C. J. Clinical practice. Vitamin D insufficiency. *N. Engl. J. Med.* **364**, 248–254 (2011).
- Holick, M. F. Sunlight and vitamin D for bone health and prevention of autoimmune diseases, cancers, and cardiovascular disease. *Am. J. Clin. Nutr.* **80**, 1678S–1688S (2004).
- Ciardullo, S. et al. Low 25 (OH) vitamin D levels are associated with increased prevalence of nonalcoholic fatty liver disease and significant liver fibrosis. *Diabetes Metab. Res. Rev.* **39**, e3628 (2023).
- Arai, T. et al. Association of vitamin D levels and vitamin D-related gene polymorphisms with liver fibrosis in patients with biopsy-proven nonalcoholic fatty liver disease. *Dig. Liver Dis.* **51**, 1036–1042 (2019).
- Ji, Y., Wei, C. B., Gu, W. & Hou, L. L. Relevance of vitamin D on NAFLD and liver fibrosis detected by vibration controlled transient elastography in US adults: a cross-sectional analysis of NHANES 2017–2018. *Ann. Med.* **55**, 2209335 (2023).
- Kitson, M. T. & Roberts, S. K. D-livering the message: the importance of vitamin D status in chronic liver disease. *J. Hepatol.* **57**, 897–909 (2012).
- Petta, S. et al. Low vitamin D serum level is related to severe fibrosis and low responsiveness to interferon-based therapy in genotype 1 chronic hepatitis C. *Hepatology* **51**, 1158–1167 (2010).
- Terrier, B. et al. Low 25-OH vitamin D serum levels correlate with severe fibrosis in HIV-HCV co-infected patients with chronic hepatitis. *J. Hepatol.* **55**, 756–761 (2011).
- Abramovitch, S. et al. Vitamin D inhibits proliferation and profibrotic marker expression in hepatic stellate cells and decreases thioacetamide-induced liver fibrosis in rats. *Gut* **60**, 1728–1737 (2011).
- Abramovitch, S. et al. Vitamin D inhibits development of liver fibrosis in an animal model but cannot ameliorate established cirrhosis. *Am. J. Physiol. Gastrointest. Liver Physiol.* **308**, G112–G120 (2015).
- Shibamoto, A. et al. Vitamin D deficiency exacerbates alcohol-related liver injury via gut barrier disruption and hepatic overload of endotoxin. *J. Nutr. Biochem.* **122**, 109450 (2023).
- Pike, J. W. & Meyer, M. B. The vitamin D receptor: new paradigms for the regulation of gene expression by 1,25-dihydroxyvitamin D(3). *Endocrinol. Metab. Clin. North. Am.* **39**, 255–269 (2010).

24. Chen, K. S. & DeLuca, H. F. Isolation and characterization of a novel cDNA from HL-60 cells treated with 1,25-dihydroxyvitamin D-3. *Biochim. Biophys. Acta* **1219**, 26–32 (1994).
25. Santos, P. P. D. et al. Vitamin D Supplementation Induces Cardiac Remodeling in Rats: Association with Thioredoxin-Interacting Protein and Thioredoxin. *Arq. Bras. Cardiol.* **116**, 970–978 (2021).
26. Kim, Y. et al. Thioredoxin-interacting Protein (TXNIP) Mediates Thioredoxin-dependent Antioxidant Mechanism in Endometrial Cancer Cells Treated With 1 α ,25-dihydroxyvitamin D(3). *Anticancer Res.* **39**, 4795–4803 (2019).
27. Hamilton, J. P., Potter, J. J., Koganti, L., Meltzer, S. J. & Mezey, E. Effects of vitamin D3 stimulation of thioredoxin-interacting protein in hepatocellular carcinoma. *Hepatol. Res.* **44**, 1357–1366 (2014).
28. Park, H. S. et al. TXNIP/VDUP1 attenuates steatohepatitis via autophagy and fatty acid oxidation. *Autophagy* **17**, 2549–2564 (2021).
29. Jung, E. et al. TXNIP in liver sinusoidal endothelial cells ameliorates alcohol-associated liver disease via nitric oxide production. *Int. J. Biol. Sci.* **20**, 606–620 (2024).
30. Mariotti, V. et al. Animal models of cholestasis: An update on inflammatory cholangiopathies. *Biochim. Biophys. Acta Mol. Basis Dis.* **1865**, 954–964 (2019).
31. Gascon-Barre, M. et al. The normal liver harbors the vitamin D nuclear receptor in nonparenchymal and biliary epithelial cells. *Hepatology* **37**, 1034–1042 (2003).
32. Gonzalez-Sanchez, E., Firrincieli, D., Housset, C. & Chignard, N. Expression patterns of nuclear receptors in parenchymal and non-parenchymal mouse liver cells and their modulation in cholestasis. *Biochim. Biophys. Acta Mol. Basis Dis.* **1863**, 1699–1708 (2017).
33. Ding, N. et al. A vitamin D receptor/SMAD genomic circuit gates hepatic fibrotic response. *Cell* **153**, 601–613 (2013).
34. Wang, P. et al. Vitamin D receptor attenuates carbon tetrachloride-induced liver fibrosis via downregulation of YAP. *J. Hazard. Mater.* **478**, 135480 (2024).
35. Dong, B. et al. Vitamin D Receptor Activation in Liver Macrophages Ameliorates Hepatic Inflammation, Steatosis, and Insulin Resistance in Mice. *Hepatology* **71**, 1559–1574 (2020).
36. Malone, C. F. et al. mTOR and HDAC Inhibitors Converge on the TXNIP/Thioredoxin Pathway to Cause Catastrophic Oxidative Stress and Regression of RAS-Driven Tumors. *Cancer Discov.* **7**, 1450–1463 (2017).
37. Stokes, C. S., Volmer, D. A., Grunhage, F. & Lammert, F. Vitamin D in chronic liver disease. *Liver Int.* **33**, 338–352 (2013).
38. Wang, J. et al. 1 α ,25-Dihydroxyvitamin D(3) inhibits aflatoxin B1-induced proliferation and dedifferentiation of hepatic progenitor cells by regulating PI3K/Akt and Hippo pathways. *J. Steroid Biochem. Mol. Biol.* **183**, 228–237 (2018).
39. Yamaguchi, F. et al. Rare sugar D-allose induces specific up-regulation of TXNIP and subsequent G1 cell cycle arrest in hepatocellular carcinoma cells by stabilization of p27kip1. *Int. J. Oncol.* **32**, 377–385 (2008).
40. Kwon, H. J. et al. Vitamin D3 up-regulated protein 1 deficiency accelerates liver regeneration after partial hepatectomy in mice. *J. Hepatol.* **54**, 1168–1176 (2011).
41. Kwon, H. J. et al. Vitamin D3 upregulated protein 1 suppresses TNF- α -induced NF- κ B activation in hepatocarcinogenesis. *J. Immunol.* **185**, 3980–3989 (2010).
42. Kato, S. The function of vitamin D receptor in vitamin D action. *J. Biochem.* **127**, 717–722 (2000).
43. Xie, J. et al. Yes-associated protein regulates the hepatoprotective effect of vitamin D receptor activation through promoting adaptive bile duct remodeling in cholestatic mice. *J. Pathol.* **255**, 95–106 (2021).
44. Firrincieli, D. et al. Vitamin D nuclear receptor deficiency promotes cholestatic liver injury by disruption of biliary epithelial cell junctions in mice. *Hepatology* **58**, 1401–1412 (2013).
45. Boulter, L. et al. Macrophage-derived Wnt opposes Notch signaling to specify hepatic progenitor cell fate in chronic liver disease. *Nat. Med.* **18**, 572–579 (2012).
46. He, Y. H., Pan, J. X., Xu, L. M., Gu, T. & Chen, Y. W. Ductular reaction in non-alcoholic fatty liver disease: When Macbeth is perverted. *World J. Hepatol.* **15**, 725–740 (2023).
47. Gadd, V. L. et al. The portal inflammatory infiltrate and ductular reaction in human nonalcoholic fatty liver disease. *Hepatology* **59**, 1393–1405 (2014).
48. Carpino, G. et al. Macrophage Activation in Pediatric Non-alcoholic Fatty Liver Disease (NAFLD) Correlates with Hepatic Progenitor Cell Response via Wnt3a Pathway. *PLoS One* **11**, e0157246 (2016).
49. Masaki, S., Masutani, H., Yoshihara, E. & Yodoi, J. Deficiency of thioredoxin binding protein-2 (TBP-2) enhances TGF- β signaling and promotes epithelial to mesenchymal transition. *PLoS One* **7**, e39900 (2012).
50. Hanada, S., Snider, N. T., Brunt, E. M., Hollenberg, P. F. & Omary, M. B. Gender dimorphic formation of mouse Mallory-Denk bodies and the role of xenobiotic metabolism and oxidative stress. *Gastroenterology* **138**, 1607–1617 (2010).
51. Scandlyn, M. J., Stuart, E. C. & Rosengren, R. J. Sex-specific differences in CYP450 isoforms in humans. *Expert. Opin. Drug Metab. Toxicol.* **4**, 413–424 (2008).

Acknowledgements

The authors thank Dr. Yeoh from the University of Western Australia for providing us with the BMOL cell line. This work was supported by National Research Foundation of Korea (NRF) grants funded by the Korean government (MSIT) (NRF-2022R1A2C3013064 to H.K., RS-2025-00562771 to H.K., and RS-2023-00210903 to H.S.E.) and by the Korea Research Institute of Bioscience and Biotechnology (KRIBB) Research Initiative Program (KGS1022221 to Y.W.).

Author contributions

E.B.B., H.S.E., and J.S. contributed equally to this paper. E.B.B. and J.S. performed experiments, analyzed data, and prepared the manuscript. H.S.E. provided human samples and designed the experiments. E.H., S.P., P.K., S.P., and Y.C. performed experiments and analyzed data. S.K., S.O.K., and H.N.K. provided human samples. Y.W. and H.K. contributed to the design of the study; manuscript writing; administrative, technical, and material support; and study supervision. All authors have read and approved the final manuscript.

Competing interests

The authors declare no competing interests.

Additional information

Supplementary information The online version contains supplementary material available at <https://doi.org/10.1038/s41467-025-59724-z>.

Correspondence and requests for materials should be addressed to Young-Suk Won or Hyo-Jung Kwon.

Peer review information *Nature Communications* thanks Makoto Makishima and the other, anonymous, reviewer(s) for their contribution to the peer review of this work. A peer review file is available.

Reprints and permissions information is available at <http://www.nature.com/reprints>

Publisher's note Springer Nature remains neutral with regard to jurisdictional claims in published maps and institutional affiliations.

Open Access This article is licensed under a Creative Commons Attribution-NonCommercial-NoDerivatives 4.0 International License, which permits any non-commercial use, sharing, distribution and reproduction in any medium or format, as long as you give appropriate credit to the original author(s) and the source, provide a link to the Creative Commons licence, and indicate if you modified the licensed material. You do not have permission under this licence to share adapted material derived from this article or parts of it. The images or other third party material in this article are included in the article's Creative Commons licence, unless indicated otherwise in a credit line to the material. If material is not included in the article's Creative Commons licence and your intended use is not permitted by statutory regulation or exceeds the permitted use, you will need to obtain permission directly from the copyright holder. To view a copy of this licence, visit <http://creativecommons.org/licenses/by-nc-nd/4.0/>.

© The Author(s) 2025

¹College of Veterinary Medicine, Chungnam National University, Daejeon, Republic of Korea. ²Department of Physiology, College of Medicine, Jeju National University, Jeju, Republic of Korea. ³Department of Internal Medicine, School of Medicine, Chungnam National University, Daejeon, Republic of Korea. ⁴Department of Internal Medicine, Chungnam National University Hospital, Daejeon, Republic of Korea. ⁵Laboratory Animal Resource Center, Korea Research Institute of Bioscience and Biotechnology, Chungbuk, Republic of Korea. ⁶College of Pharmacy, Chungnam National University, Daejeon, Republic of Korea. ⁷Department of Surgery, College of Medicine, Chungnam National University, Daejeon, Republic of Korea. ⁸Department of Medical Sciences, Chungnam National University, Daejeon, Republic of Korea. ⁹Department of Food and Nutrition, Andong National University, Andong, Republic of Korea. ¹⁰These authors contributed equally: Eun Bok Baek, Hyuk Soo Eun, Jun-Yeop Song. ✉ e-mail: yswon@kribb.re.kr; hyojung@cnu.ac.kr